Title
Liquid-Phase Electron Microscopy for Soft Matter Science and Biology

Journal
Advanced Materials, 32(25)

ISSN
0935-9648

Authors
Wu, Hanglong
Friedrich, Heiner
Patterson, Joseph P
et al.

Publication Date
2020-06-01

DOI
10.1002/adma.202001582

ADVANCED MATERIALS
www.advmat.de

Liquid-Phase Electron Microscopy for Soft Matter Science and Biology

*Hanglong Wu, Heiner Friedrich, Joseph P. Patterson, Nico A. J. M. Sommerdijk, and Niels de Jonge**

Innovations in liquid-phase electron microscopy (LP-EM) have made it possible to perform experiments at the optimized conditions needed to examine soft matter. The main obstacle is conducting experiments in such a way that electron beam radiation can be used to obtain answers for scientific questions without changing the structure and (bio)chemical processes in the sample due to the influence of the radiation. By overcoming these experimental difficulties at least partially, LP-EM has evolved into a new microscopy method with nanometer spatial resolution and sub-second temporal resolution for analysis of soft matter in materials science and biology. Both experimental design and applications of LP-EM for soft matter materials science and biological research are reviewed, and a perspective of possible future directions is given.

1. Introduction

Liquid-phase electron microscopy (LP-EM) is a newly accessible analytical method that has opened up a rapidly emerging field of research during the past decade.[1] Although many previous successes in LP-EM have revolved around hard materials, such as metallic nanoparticles,[2] new scientific insights are also expected from applying LP-EM to the study of key questions in soft matter science.[3] This application has been limited in the past due to various experimental difficulties, but continuous progress has brought the field to a status where it is now readily possible to directly visualize structure and examine dynamics of hydrated soft materials. Soft matter refers to a state of condensed matter that is able to undergo dynamic changes due to its physical behavior occurring at an energy scale comparable with thermal energy (kT). Typical examples of soft matter are liquids, polymers, and gels, as well as many biological materials, such as membranes and proteins. An important question in applied soft matter physics is how to control molecular systems whose manifold characteristics result from these systems being out of equilibrium.[4] Soft matter has complex interactions with its surroundings as a result of the manifold of intra- and intermolecular interactions. The interplay of enthalpic and entropic effects causes interesting phenomena, such as structural organization extending from molecular dimensions all the way to the micron scale. To control soft matter systems, more understanding is needed of nonequilibrium phenomena, such as kinetic trapping and active matter.[5] Also, having a better understanding of the interaction potentials between nanosized objects in liquid is required. Here, molecular simulations and direct imaging techniques have been proposed[6] as tools for gaining further insight into the dynamic nature of soft materials.

The technique of LP-EM is still in an early stage, and many of the papers in the field involve studies of the technique itself, while it is not yet always clear what new scientific insights can be obtained due to interference of electron-beam effects with the observables.[7] Setting purely technical developments aside, the main challenge in the field is how to understand, control, and in some cases use the electrochemical interactions that takes place as the high-energy electron beam penetrates the sample. Thus, a critical evaluation is needed to address the questions of what information LP-EM has provided about materials systems

H. Wu, Dr. H. Friedrich
Department of Chemical Engineering and Chemistry
Eindhoven University of Technology
Eindhoven 5600 MB, The Netherlands
Dr. H. Friedrich
Institute for Complex Molecular Systems
Eindhoven University of Technology
Eindhoven 5600 MB, The Netherlands
Prof. J. P. Patterson
Department of Chemistry
University of California
Irvine, CA 92697, USA
Prof. N. A. J. M. Sommerdijk
Department of Biochemistry
Radboud University Medical Center
Nijmegen 6500 HB, The Netherlands
Prof. N. de Jonge
INM – Leibniz Institute for New Materials
Saarbrücken 66123, Germany
E-mail: niels.dejonge@leibniz-inm.de
Prof. N. de Jonge
Department of Physics
Saarland University
Saarbrücken 66123, Germany
The ORCID identification number(s) for the author(s) of this article can be found under https://doi.org/10.1002/adma.202001582.

DOI: 10.1002/adma.202001582

and biological samples. Second, as even weak perturbations can lead to significant changes in the sample, experiments need to be performed with highly optimized protocols. Moreover, standardization of the reported experimental details in LP-EM is needed, since a lack of details on the experiments may result in poor reproducibility, which is an issue currently limiting progress in this field. Finally, we hope to inspire researchers in the soft matter community to take advantage of and further develop this new and exciting methodology for solving grand challenges in soft matter research.

2. Observing Soft Matter in Liquid: Methods and Considerations

This section will address key experimental aspects of LP-EM, and in particular electron dose considerations, since soft matter is typically sensitive to radiation damage. An overview of the different available experimental systems will be given, and several practical guidelines for the experiments will be provided, including a recommendation for detailed reporting.

2.1. Analyzing Beam-Sensitive Samples with LP-EM

Generally formulated, electron microscopy probes the local charge density of a sample. Electron-beam interaction with a sample results in both elastic and inelastic electron scattering, and henceforth changes of three measurable properties of the transmitted beam: trajectory, phase, and energy. Contrast in images is obtained mostly from elastic scattering resulting in angular deviations of the electron trajectories (particle nature) and changes in phase of the electron wave (wave nature). Inelastic scattering is mostly unwanted when imaging radiation-sensitive samples since energy loss of the electron beam causes radiation damage,[8] even though inelastic scattering is useful for elemental analysis. Soft matter in solution is especially prone to radiation effects during electron microscopy as the involved binding energies are low, comparable with room temperature thermal energy (kT). Of particular importance for successful LP-EM experiments is thus a fundamental understanding of electron-beam–sample interactions, and an optimal choice of experimental settings for reducing radiation damage.

2.1.1. Radiation Damage

Beam–sample interactions are divided into two classes: dynamic processes and destructive, irreversible events. Dynamic processes include the creation of heat, excited states, and charge pairs that are reversible, while irreversible events include the breakage of chemical bonds and knock-on damage.[9] The extent of beam damage observed in the sample is typically proportional to the total electron dose received by the sample via destructive events, while reversible processes have an additional dependency on the electron flux. Therefore, the application of low electron flux may be used to mitigate radiation damage in case of reversible processes, leaving time for the sample to equilibrate heat, charge pairs, and charge separation.[10]

Hanglong Wu received his M.S. at Zhejiang University, China (2016) and then he joined the Marie Curie Innovative Training Network "MULTIMAT" as a Ph.D. fellow. He is now a 4th year Ph.D. student at Eindhoven University of Technology (Netherlands). His research focuses on using low-dose liquid-phase TEM and cryogenic TEM to study beam-sensitive materials.

Heiner Friedrich received his Ph.D. in inorganic chemistry from Utrecht University, Netherlands in 2009. He is now assistant professor in the Laboratory of Physical Chemistry of Eindhoven University of Technology, where he also leads the electron microscopy unit of the Department of Chemical Engineering and Chemistry. His research focuses on morphology evolution and optimization in multiscale materials built from, e.g., silica/silicates or graphene using quantitative imaging approaches.

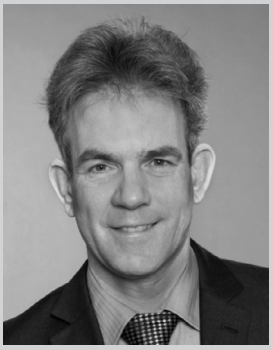

Niels de Jonge received his master's degree in physics from the University of Amsterdam, Netherlands (1994), and his Ph.D. in biophysics from the University of Freiburg, Germany (1999). He worked at Philips Research, Netherlands (2000–2005). He pioneered liquid-phase electron microscopy at Oak Ridge National Laboratory (2005–2010), while also an assistant professor at Vanderbilt University School of Medicine (2007–2011). Currently, he is senior group leader at the INM – Leibniz Institute for New Materials, Germany (2012–present), and honorary professor of physics at Saarland University.

For a detailed description of beam effects, the different constituents of the sample and the liquid enclosure need to be considered. In the case of a liquid cell filled with water, electron beam–water interaction will lead to a radiolytic plume and cascading reactions. These reactions produce hydroxyl radicals, hydrogen ions, and solvated electrons that will locally change the solution chemistry, e.g., change the pH of the

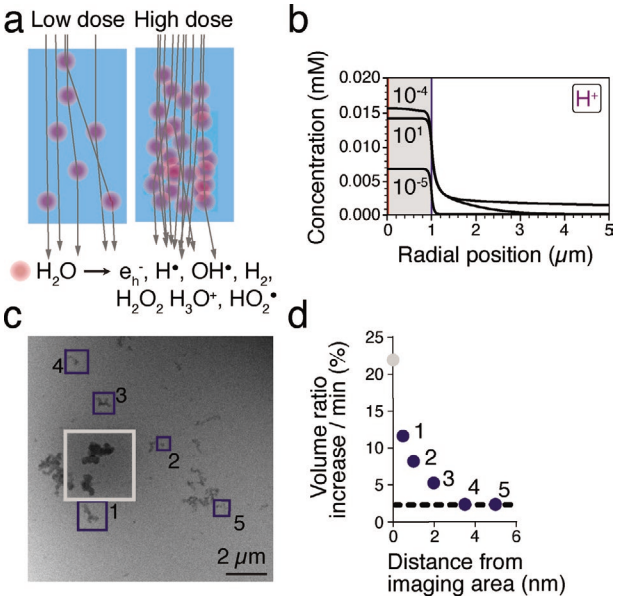

Figure 1. Electron beam–water interaction. Chemical gradients created by electron beam exposure, subsequent radiolysis, and outward diffusion of radiolysis products. a) Schematic representation of electron beam–water interactions on the nanometer scale. At high electron doses, plumes start to overlap, which can lead to changes in the concentration of radiolytic species as compared to the low-dose situation where plumes do not overlap.[10c] b) Simulations in pure water for H^+ gradients at the edge of the illuminated area and at different electron fluxes.[11a] c) Low magnification of BF STEM overview after reaction showing acquisition area (white square) and cobalt carbonate particles (blue squares) that have grown at different rates during electron beam exposure.[12] d) Volume growth dependent on distance to edge of illuminated area.[12] b) Reproduced with permission.[11a] Copyright 2014, American Chemical Society (ACS). c,d) Reproduced with permission.[12] Copyright 2019, ACS.

liquid (**Figure 1**a,b).[10c,11a,b] These effects depend on the type of microscopy modality used, i.e., transmission electron microscopy (TEM), scanning transmission microscopy (STEM), or scanning electron microscopy (SEM), as well as on the dose, the electron flux, the time after first electron impact, and the beam energy. Additionally, these effects will lead to chemical gradients in the liquid, especially at the edges of the illuminated area as shown both by computer modeling (Figure 1b)[11a] and experiment (Figure 1c,d).[12] Most interactions between electrons and water originate from plasmon loss at 25 eV as shown by electron energy loss spectroscopy (EELS).[13]

Most experiments will not involve pure water but rather a saline, and so the involved electrochemistry in the liquid is even more complex. For example, gold nanoparticles were observed to move, agglomerate, or dissolve upon electron-beam irradiation depending on the salt concentration, and the pH set by a buffer.[14] Moreover, a range of experiments involves other liquids than water. Detailed knowledge of the involved chemical reactions would be needed for design and interpretation of LP-EM experiments, as is available at least in theory for pure water.[11a]

In most TEM and STEM experiments, the electron-beam-induced temperature rise in liquid is estimated to be negligible (less than a few degrees Celsius) due to the high heat capacity and thermal conductivity of water.[15] Nevertheless, it should be accounted for when studying temperature-sensitive samples. It is also important to note that the local temperature change may become more significant if a focused intense beam is applied.[15b]

The electron beam will also change the objects in the liquid, mostly via ionization in soft matter, which may lead to the breaking of bonds (e.g., bond scission in dissolved aqueous polystyrene sulfonate[16]) and/or the disintegration of the structure[9] (e.g., shrinkage of bacterial cells[17]). Also, the objects may become electrically charged, and at high electron dose and high beam energy, knock-on damage directly removing atoms from material will play a role.

The enclosing windows of the liquid cell are also affected by the electron beam. For example, it has been reported that a positive surface potential is developed by electron-beam exposure of insulating TEM foils,[18] and also silicon nitride (SiN) often used as window material becomes positively charged,[19] leading to local electric fields influencing the sample in the liquid directly at the window.[20] Moreover, electron scattering in the window material also leads to the creation of free electrons that may damage the sample. Beam-window effects generally can be neglected when graphene is used as window material.[21]

2.1.2. Chemical Biasing

In the context of electron-beam effects, it is also important to consider the possibility of rationally using the electron beam to initiate chemical reactions in the liquid sample[22] as is frequently done to start growth processes of metallic nanoparticles.[23] It has been shown that concentrations of primary radiolysis products depend on electron flux, dissolved gasses,[11a] organic molecules,[11a] and even metal ions.[24] Irradiating pure water will typically create a reducing environment for the metallic ions, but nevertheless, oxidation of organic molecules is expected to take place due to the high reactivity of generated hydroxyl radicals. Simulations for pure water indicated that the pH will be reduced,[11a] but the pH may increase in the presence of other solutes which the model did not account for, such as cerium ions.[25] Utilizing these electron-beam effects is an option for controlling the behavior and properties of soft matter in a liquid cell. An example is an experiment in which the formation of micelles from a poly(polyethylene)glycol macro chain transfer agent was initiated by homolytic cleavage of the trithiocarbonate group followed by an addition of a hydrophilic chain, resulting in a block co-polymer structure that underwent a microphase separation in water.[26] Micelle formation was induced by continuous exposure to an electron flux of 0.5 e^- $Å^{-2}$ s^{-1}, and it was assumed that the contribution from radicals created from radiolysis of water was negligible as long as sufficiently high monomer concentrations were used. Electron-beam control of an experiment thus seems feasible as long as the electron flux is kept to a minimum. However, to support predictions concerning the changes in the chemical environment within the liquid cell, a detailed simulation of the chemical conditions would be helpful.

2.1.3. Defining and Testing the Acceptable Dose Level

The aforementioned considerations about radiation damage pose the fundamental question of how to define acceptable

electron dose levels for a given system. Doses of even less than 1 e Å^{-2} can induce significant changes in the ultrastructure of intact bacterial cells,[17,27] and have been reported to change the structure of proteins.[28] The requirements of the experiment must be determined in terms of preservation of either: i) the morphology of the sample[29] or ii) the native reaction kinetics[12,30] whereby the reaction can be a chemical reaction,[12] a self-assembly process,[3b,31] etc.

Here, we can learn from the advances in cryogenic TEM (cryo-TEM and of course also cryo-STEM), where electron-beam effects have been extensively investigated as they crucially determine the obtainable resolution in the structure analysis of biological specimens.[32] The limiting electron dose for a specific system can be determined from the dose-dependent disappearance of diffraction peaks,[32b] or Fourier-transferred signals,[33] whereby such peak or signal typically reduces in intensity exponentially with the electron dose. The electron exposure at which the intensity of the component decreases to a factor of e^{-1} (≅0.4) below its initial value is defined as the critical exposure.[34] Importantly, the loss of structural information is resolution-dependent: high-resolution details in a specimen are lost first while low-resolution features are retained up to significantly higher electron doses.[32c] This approach has also been applied in LP-EM,[10b,28] and can be used to set the optimal electron dose for a given required resolution.

Hence, to evaluate dose effects in LP-EM experiments, we recommend recording a series of images of which the initial ones represent the lowest possible dose in an overview image. Dose effects can be assessed by comparing structures and processes at different doses, electron fluxes, or even different beam energies.[30,35] In case of reaction kinetics, one should aim to determine if the zero-dose and non-zero-dose observations actually match[15c] or, even better, extrapolate the observed differences in reaction/assembly dynamics to a zero-electron flux.[12] The latter approach was successfully used to experimentally confirm the theoretically predicted chemical gradients present at the edges of the illuminated region by quantifying differences in growth rate as dependent on the distance to the edge (Figure 1c,d).

Ideally, the chemical composition of the sample should be probed after electron beam irradiation. A "post mortem" analysis (not in liquid) is possible using matrix-assisted laser desorption ionization imaging mass spectrometry (MALDI-IMS), a technique for providing spatially resolved chemical information with less than 100 µm resolution, to study the beam effects on both linear and cyclic peptide sequences.[31] As the resolution of MALDI-IMS is on the order of the window size, it is possible to directly monitor the degradation of the peptide sequences after imaging and disassembly of the cell. Damage thresholds were determined by varying electron flux, accumulative electron flux, and using pulsed (1 s) or continuous exposure. The accumulative electron flux thresholds were ≈10^2–10^3 e^- Å^{-2}, but varied for the linear and cyclic versions, and increased for pulsed experiments. Moreover, it was shown that even when imaging at fluxes resulted in complete degradation of the peptide, self-assembled structures would appear in the liquid cell, cautioning against interpretation of data where electron–sample interactions are not established.

2.1.4. Adjusting an Experiment to the Required Resolution

For every experiment, a balance needs to be found between the minimum electron dose and electron flux on the one hand, and the required spatial and temporal resolution on the other hand. It is important to note that the highest possible resolution set by the electron optics, which is at the Ångstrom level in modern electron microscopes, will typically not be achieved because of the radiation sensitivity of the materials. An important consideration prior to the experiment is to determine what resolution is needed to address a specific research question, and to optimize the experiment accordingly. The achievable dose-limited resolution δ, namely, is highly sensitive to the total accumulated dose D via the following scaling law[1g,9,36]

$$\delta \sim D^{-a} \tag{1}$$

whereby the exponent ranges from $a = 0.25$[36] to $a = 0.5$[9] depending on how the objects in the liquid are accounted for in the calculation. This scaling law implies that relaxing the resolution level of an experiment may thus be highly beneficial. Note that D, traditionally used in the field of electron microscopy, is defined as electrons per unit area, which is in fact the electron density, and differs from the concept of dose in radiation biology, which is the absorbed dose per unit mass of the irradiated object.

2.1.5. Methods to Optimize the Information Obtained

Experiments should be performed with optimized settings in order to maximize the amount of information obtained per electron. To enable such optimization, the image quality needs to be determined in a quantitative way, which is typically, characterized in terms of the resolution achieved at sufficient signal-to-noise ratio (SNR).[27,37,43] Using the Rose criterion, this means that for a feature to be detectable in an image, the signal above background should be a factor of three larger than the background fluctuations (noise).[38]

Analytical and numerical approaches have been developed to calculate the resolution obtained in liquid layers for both STEM,[1a,1g,36,39] TEM,[1a,1g,36,40] and SEM.[1a] Theoretical predictions have been mostly verified by experimental work, and there is a good understanding of the imaging parameters in liquid,[29a] ice,[41] and related systems.[37,43] Optimization of imaging parameters for STEM is effectively done by numerical simulations.[37,42,43] For example, the settings for optimal SNR are readily calculated as a function of D (**Figure 2**a).[37] While single pixel estimation of the SNR[37] or resolution[36] can be sufficient for optimizing the imaging parameters, dedicated Monte Carlo software such as Casino[42] also allows simulation of image data of complex sample geometries as was demonstrated for LP-EM of yeast cells (Figure 2b–d).[27] The resolution in TEM can be calculated using analytical equations of beam blurring and energy broadening, which are the dominating factors limiting the resolution, and match the experiment.[1g,43] The resolution of SEM is obtained from evaluating beam broadening through the liquid separating window in case of backscatter detection and through the sample thickness and window in case of transmission mode.[1a]

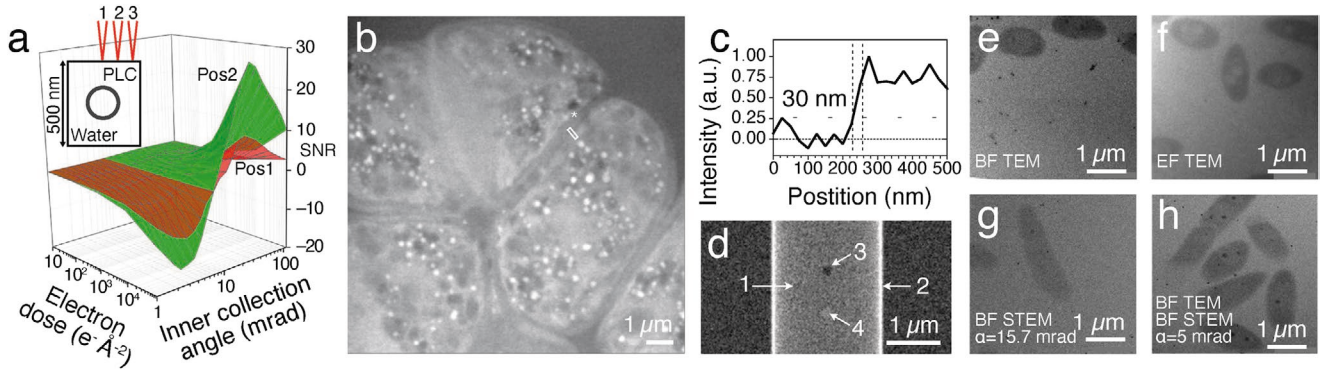

Figure 2. Finding optimal imaging settings for LP-EM of soft matter. a) Simulating the SNR of a polymeric micelle in 500 nm of water. The red arrows illustrate three different positions analyzed: 1) center of the micelle, 2) edge of the micelle, and 3) liquid background. An expert map is presented where the SNR at micelle locations (1) and (2) is plotted as a function of electron dose and inner collection angle. Negative and positive SNR values relate to BF-STEM, and ADF STEM, respectively. For maximum SNR, the expert map suggests using an inner collection angle 2–3 mrad for BF-STEM and 20–30 mrad inner collection angle for ADF-STEM when imaging polymeric micelle in liquid with the α set to 5 mrad. b) Unstained yeast cells in liquid imaged with ADF STEM. c) The obtained spatial resolution amounted to 30 nm. d) A Monte Carlo image simulation performed with the Casino software was used to understand the contrast mechanism and resolution. e–h) Different electron microscopy modalities and parameters were compared for imaging intact bacterial cells in 300–400 nm of liquid. BF-TEM resulted in a factor of three better SNR than BF-STEM, and EF TEM, using a 30 eV slit placed at the zero-loss peak, resulted in much better SNR than BF-STEM. The electron flux amounted to 1 e^{-} $Å^{-2}$ s^{-1}. a) Reproduced under the terms of the CC-BY Creative Commons Attribution 4.0 International License (http://creativecommons.org/licenses/by/4.0/).[37] Copyright 2018, The Authors, published by the Royal Society. b–d) Reproduced with permission.[27] Copyright 2011, Elsevier. e–h) Adapted with permission.[29a] Copyright 2019, Elsevier.

2.1.6. TEM

Another important question is which microscopy modality to use. TEM is the most used imaging modality in LP-EM (**Figure 3**a). In TEM, a uniform, circular illumination area is projected on the sample. The transmitted electrons are collected by the objective lens and detected by the pixelated sensor of the camera. This setup has several advantages. Detection is via phase contrast in the case of thin samples, providing the best possible balance between spatial resolution and electron dose.[9] In dynamic experiments, high temporal resolution up to millisecond frame times can be obtained.[1g] However, in samples thicker than one half of the mean-free-path-length of elastic electron scattering (≈160 nm for water at 200 keV beam energy),[36] phase-contrast TEM becomes blurred and the resolution-limiting factor in TEM is the chromatic aberration C_C of the objective lens. The effect of chromatic aberration decreases the spatial resolution in TEM from 0.2 to 5 nm due to the 30 eV energy spread ΔE gained by the electron-beam transmitting through a water layer of a typical thickness encountered in LP-EM experiments.[1g]

Energy-filtered TEM (EF-TEM) may be used to reduce the energy distribution of the transmitted beam and hence mitigates the effect of chromatic aberration, but fewer electrons are then available for detection. For example, energy filtering improved the SNR of bacterial cells imaged in 300–400 nm of liquid (Figure 2e,f).[29a] Chromatic aberration correction can be used to maintain a high spatial resolution, even for thick samples, maintaining as many electrons as possible for detection.[44]

2.1.7. STEM and SEM

In STEM and SEM, the specimen is scanned by a focused electron probe. In STEM (Figure 3b), the transmitted electron intensity at each location is recorded directly by an annular detector. STEM does not need a post-specimen objective lens, which is the main source of resolution-limiting chromatic aberration in TEM. Annular dark-field (ADF) STEM is particularly effective for imaging materials of high atomic number in thick liquid layers due to the strong dependence of its contrast on atomic number. In terms of the SNR and obtainable resolution, this offers an important advantage in micrometer-thick specimens as has been shown experimentally for imaging gold nanoparticles in water of micrometers-thick liquid.[1a,45] Nanometer resolution of soft matter is obtained[46] with STEM detection for such thick samples containing high-Z nanoparticles.[47]

SEM of liquid specimens (Figure 3c) is mostly operated using backscatter detection, but then the resolution is on the order of 10 nm for high-Z materials and up to several tens of nanometers for low-Z materials due to lower efficiency of backscatter detection.[1a,48] Using STEM detection in SEM improves the resolution to 3–4 nm for high-Z labels.[46]

2.1.8. Choosing between TEM, STEM, or SEM

Theoretical and experimental studies indicate that TEM phase contrast outperforms the resolution of STEM for low atomic number materials (e.g., biological cells) when imaging in liquid or ice with a thickness of up to 200 nm.[36,49] For thicker samples of low atomic number, bright field STEM (BF-STEM) provides better resolution, while samples that also contain objects of higher atomic number, e.g., gold nanoparticles used as protein labels, are most efficiently imaged with ADF STEM.[1g,36] By direct comparison of different imaging modalities applied to intact bacterial cells in liquid, BF-TEM and EF-TEM were both found to exhibit a higher SNR than BF-STEM, whereby the EF-TEM increased the SNR compared to BF-TEM (Figure 2e–h).[29a] The microscopy method also differs in the way the dose will be

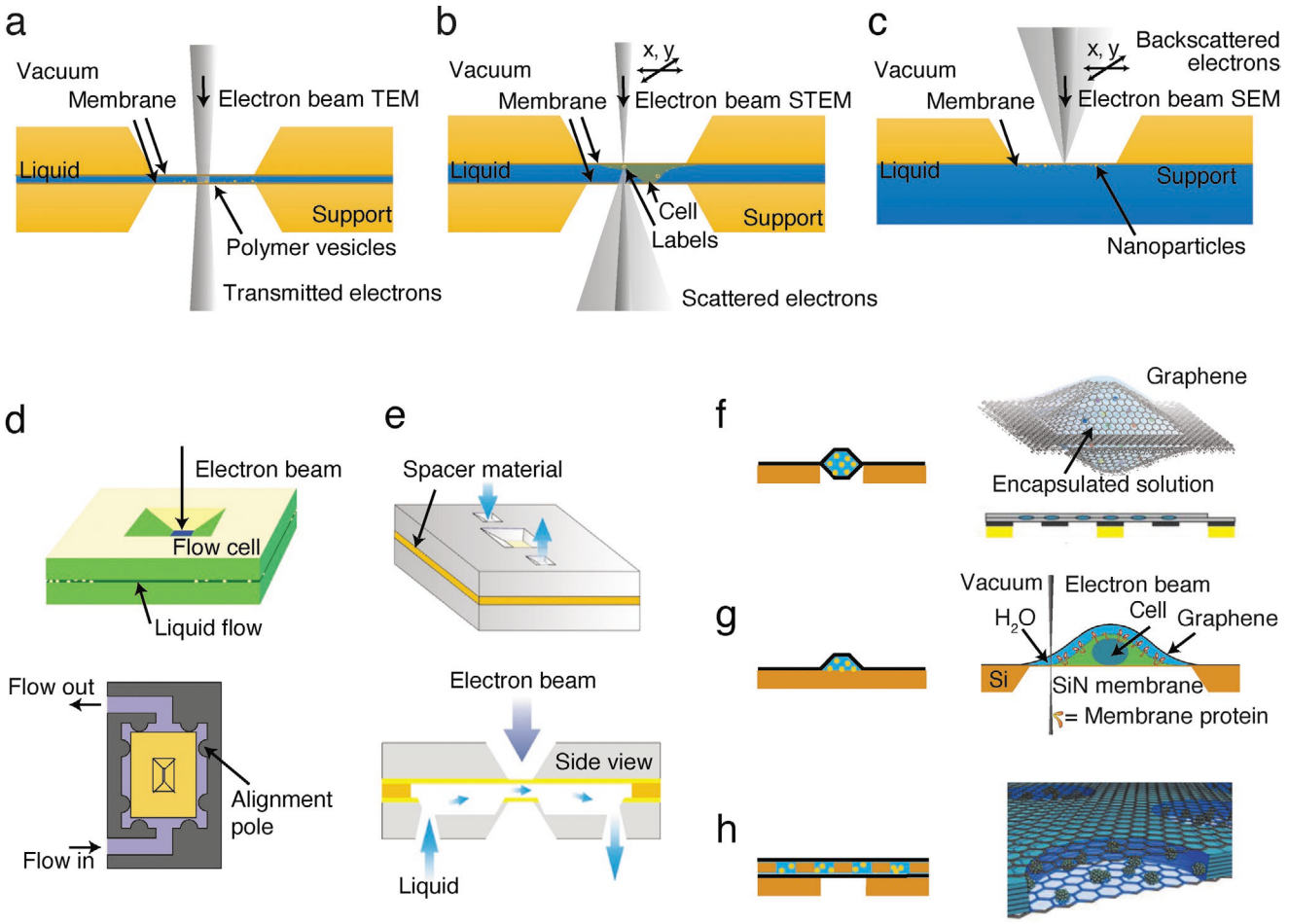

Figure 3. Experimental configurations for LP-EM. a) A sample enclosed in a liquid cell consisting of two silicon microchips supporting silicon nitride (SiN) windows. The stationary beam of EM is used to study objects, e.g., polymer vesicles in a thin liquid layer, preferably at the beam exit window. b) The focused scanning electron probe of STEM achieves the highest resolution for objects at the beam entrance window, it is particularly efficient for detecting labels in micrometers-thick liquid. c) SEM in a configuration with backscatter detection through a liquid-vacuum separating membrane. d) A flow cell consisting of two microchips with liquid flow between them (top). A bypass flow is effectively formed by liquid flowing around the microchips (bottom). The microchips are placed in a slot and their position steered via alignment poles. e) Direct flow cell containing a flow path through the microchips, thus avoiding liquid flow around the windows. f). Small liquid pockets are obtained by sandwiching two sheets of graphene providing the thinnest possible liquid cell. g) A single layer of graphene can be used to coat a sample, e.g., a eukaryotic cell immobilized on a SiN substrate for protection against evaporation of the liquid. h) Graphene can also be used to enclose liquid pockets defined by a substrate with holes containing liquid. a–c) Adapted with permission.[1a] Copyright 2011, Springer Nature. d) Top panel: Adapted with permission.[1a] Copyright 2011, Springer Nature. Bottom panel: Reproduced with permission.[50] Copyright 2010, Cambridge University Press. e) Adapted with permission.[51] Copyright 2013, ACS. f) Left panel: Reproduced with permission.[21] Copyright 2018, ACS. Right panel: Adapted with permission.[23] Copyright 2012, American Association for the Advancement of Science (AAAS). g) Left panel: Reproduced with permission.[21] Copyright 2018, ACS. Right panel: Reproduced with permission.[52] Copyright 2017, ACS. h) Left panel: Reproduced with permission.[21] Copyright 2018, ACS. Right panel: Reproduced under the terms and conditions of the ACS AuthorChoice/Editors' Choice CC-BY Creative Commons Attribution 4.0 International Public License (https://pubs.acs.org/page/policy/authorchoice_ccby_termsofuse.html).[53] Copyright 2018, ACS.

applied, and this aspect needs to be considered as well. STEM differs from TEM in the sense that the total current applied to the sample is much lower, which may be advantageous for some experiments. Conversely, to avoid edge effects due to radical diffusion, a homogenously "altered" solution chemistry with an illuminated area much larger than the field of view of the detector (CCD camera) may be more easily achieved in TEM. SEM is used when a resolution[1a,46] of 4–10 nm is sufficient with the advantage that larger samples can be studied than with TEM and STEM, but due to the lower beam energies (≤30 keV) used, typically more beam damage is obtained in SEM than for TEM or STEM typically operating in the range of 60–300 keV.

2.1.9. Diffraction

Instead of direct imaging, it is also possible to examine samples via diffraction techniques. In particular for crystalline material, diffraction techniques require a much lower dose than direct imaging because the total dose can be divided over a much larger area. An example of analysis via diffraction has been published already in the early 1970s. A hydrated catalase crystal was studied using an environmental chamber in TEM, and spatial frequencies as small as ½ Å were observed.[28] Diffraction is currently not used in LP-EM research, presumably because conventional diffraction methods do not allow for studying

single objects and prevent dynamics. Another drawback is the requirement of a thin liquid layer (<200 nm) so as to maintain the coherence of the electron beam. Studying protein crystals in liquid is nevertheless a viable option, and would allow examining structure under various liquid conditions.

2.1.10. How to Measure the Dose

To determine the total dose D in an experiment, the following equation is typically used

$$D = \frac{I_p t}{eA} \tag{2}$$

with probe current I_p, exposure time t, area exposed to the electron beam A, and elementary charge e. For TEM, a camera with a known conversion factor of signal intensity to electron count (k_e) can be used to measure I_p. An estimate of the k_e can usually be obtained from the manufacturer; however, k_e is dependent on the acceleration voltage and will also change over time due to contamination or damage on the scintillator. In both STEM and TEM, I_p can be measured directly by using a current meter with picoampere sensitivity connected to a Faraday cup that has been built into the tip of a holder or mounted in the microscope as is the case for instruments with a post-column electron energy loss spectrometer.[54] A third option is the fluorescent screen of the microscope that is typically read-out by the system to obtain a value for the "exposure;" however, this value may not be accurate due to secondary electron generation at the phosphor screen.

2.1.11. Need for Detailed Reporting

The beam sensitivity of soft matter requires that experimental protocols are designed in such a way that all details of the LP-EM experiments are reported, preferably via a standardized procedure in a lab. When the experimental challenges of LP-EM are not discussed in detail, false expectations may be set about its applicability.[55] The imaging conditions, such as the applied dose and electron flux have a strong influence on the experiment, as well as the exact liquid conditions. For example, the salt concentration and pH can determine which nanostructures form, but those conditions are often not reported.[12,14,35a] Moreover, a dose mitigation effect was observed at low electron flux,[10b] and the waiting time between recording images may influence the observed structures and process in case of an reversible beam effect. An example emphasizing the importance of exact experimental detail is that the time elapsed between plasma cleaning of a SiN window and conducting an experiment can critically determine the outcome.[56]

Another important aspect to note and report is the "dose history" of the sample.[17] Ideally, the sample is irradiated only when data are recorded, but in practice, unintentional and often unreported irradiation occurs when searching for suitable imaging areas and adjusting the microscope settings. Low-dose techniques can be used to adjust the microscope settings at a different location than the imaged object in the sample. But this remedy does not guarantee the absence of radiation effects since reactive species created at one location may diffuse throughout the entire sample volume.

Of particular importance is to consider unreported electrons obtained during image acquisition originating from the deadtime in the measurements, which is the time that the system is not capable of recording data between measurements. In TEM, transfer of information from the camera sensor to the memory creates deadtime, as well as resetting the camera for a new acquisition. In STEM, deadtime results from the time delay between scanning two lines in which the scanning coils steer the electron beam back to the starting position. Deadtime exposure is of particular concern when acquiring time-lapse image series in LP-EM. The usage of a synchronized sub-second pre-specimen shutter, also referred to as beam blanker, can reduce the unwanted irradiation as the beam will be blanked unless the camera is recording. In STEM, overhead exposure can be mitigated by shutting off the beam during the so-called beam fly back period using a synchronized millisecond electrostatic shutter. Yet, in most experiments, there will be at least some level of beam exposure with electrons that are not being used for data collection. Hence, a dose history tool should be included in the data acquisition software tracking the entire exposure of any sample, and the information should be attached to the metadata of acquired micrographs.

2.1.12. Measuring the Liquid Thickness

Another important factor to consider for the LP-EM experiments is the liquid thickness. Electron scattering in liquid determines the background level, and thereby the achievable spatial resolution, since the resolution is typically limited by SNR in LP-EM. Also, the liquid thickness affects beam-induced effects as the amount of deposited energy per exposed area depends on the thickness.[8] Furthermore, reactions in a liquid cell may depend on the depletion of reactants in the confined volume, through which the thickness of the liquid layer may influence the reaction kinetics or morphology of growing structures.[17,57] In cases where a flow configuration is used, the separation between liquid cell walls can also affect the flow resistance and the mass-transport in the liquid cell as a result.[50] Thus, measuring *and* reporting the liquid thickness is of key importance for the interpretation of data and for being able to reproduce the results.

Generally speaking, two principal methods exist for determining the local sample thickness in electron microscopy:[45,58] 1) measuring the fraction of transmitted electrons versus incoming electrons,[9,45,59] and 2) characterization of the energy distribution of transmitted electrons, for example, via EELS.[58,60] In both cases, the measurement itself is straightforward, but estimating the absolute thickness requires calculating the scattering cross-section, which introduces the largest source of error. In particular, a linear relationship between thickness and the measured electron distribution breaks down in thick samples due to multiple scattering.[60a] The thickness of a water layer of up to 10 μm can be determined with STEM,[45] while the EELS technique can be used to measure liquid thicknesses up to 700 nm with an acceptable error level of 20%.[58,61]

When publishing papers, it is important to report details on the thickness measurement to enable reproducibility. For example, nanoscale resolution on low atomic number materials requires an exceptionally thin liquid layer and minimum window thickness that is rather difficult to achieve using a liquid cell with SiN windows,[36] and one approach, sometimes unnoticed, is to obtain high resolution at the location of a gas bubble.[62] Gas bubbles can be formed through several mechanisms, including solution radiolysis,[11b] dissolved gas in the liquid,[63] and retraction of charged water exposed to the electron beam.[64] Due to increased surface interactions, the chemistry of a hydrated surface layer under a bubble may differ from a sample fully immersed in liquid. The absolute value of the thickness is thus important to report, and is preferably measured before and after the acquisition of an image, including details of the measured quantity, the collection angle of the electron microscope, and the calculated scattering cross sections.

2.2. Instrumentation: Liquid Cell Designs and Electron Microscope Innovations

LP-EM experiments typically require a liquid enclosure or another means of separating liquid from vapor, an electron microscope, and a sample holder. Recent achievements in commercial liquid cells and custom-built systems already allow for imaging liquid specimens of low atomic number at the nanometer scale. This section provides an overview of cell designs and microscope innovations.

2.2.1. Liquid Cell Designs and Liquid Mixing

The key technical feature in LP-EM experiments is the principle by which water is introduced into the electron microscope, while avoiding evaporation due to the high vacuum in the column. Two fundamentally different liquid "enclosure" techniques have been developed, open cell and closed cell microscopy.[1a,65] The main difference between these two approaches is that the open cell requires differential pumping, obtaining a so-called environmental system in which the sample is not exposed to the high vacuum of the main microscope column. Closed cell systems employ electron-transparent membranes to encapsulate the liquid, isolating the liquid from the vacuum. The closed cell approach is most used in LP-EM today.

Both fully closed liquid cells, and liquid flow systems are available. After modern thin-film technology and microfabrication were brought to the TEM field, silicon microchips with SiN windows soon became the most popular materials for liquid cells.[66] This is mainly due to the outstanding mechanical properties of the membrane materials and the mainstream cleanroom techniques. Graphene liquid cells (GLCs) have become available in recent years as well,[21,23] but still require in-house expertise.

The broadest applicable liquid cell design should fulfill the following criteria: 1) allow simple window alignment, 2) reproducibility in obtained thin liquid layer of the desired thickness, 3) controllable mixing of solutions, 4) compatibility with elemental analysis via energy dispersive X-ray analysis (EDX) or EELS, 5) simultaneous application of heating and biasing, 6) direct measurement of solution parameters such as pH and temperature, and 7) compatibility with correlative imaging methods such as cryo-TEM and fluorescence microscopy. The existing liquid cells already partially meet these requirements, but each design also has its limitations (**Table 1**).

Table 1. The properties of different liquid cells including GLC.

Liquid cell	Flow cell		Static cell	
	Bypass flow	Direct flow	Glued cell	GLC
Preparation time	medium[a)]	medium[a)]	medium[a)]	long[a)]
Flow control	✓	✓	×	×
Initiation of the reaction in the cell	✓[b)]	✓[b)]	×[b)]	×[b)]
Resolution	medium	medium	medium	High
EDX	Δ[c)]	Δ[c)]	Δ[c)]	✓
Electron diffraction	Δ[d)]	Δ[d)]	Δ[d)]	✓
Heating and biasing capabilities	✓	✓	×	×
Reducing radiation damage	×	×	×	✓
Reproducibility of experiments	High	high	medium	Low
Compatibility with standard TEM holders	×	×	✓	✓
Commercial availability	✓	✓	✓	×
Cost	high[e)]	high[e)]	medium	Low
Reuse	×	Δ	×	×

[a)]Preparation time includes the time for sample loading, alignment, and sealing of the cell, and leak test; [b)]Electron-initiated radiolytic reaction is excluded; [c)]Depends on both the window open angle of the cell and lid of the holder tip (Δ is case dependent); [d)]Relies mainly on the thickness of the liquid (Δ is case dependent); [e)]Special TEM costs are included.

2.2.2. Flow Cells

The typical design for a closed cell consists of two face-to-face paired silicon chips and a spacer material (50 nm to 10 µm, on one of the chips) between them. The spacer is designed to define a flow path guiding the liquid flow, and sets the liquid thickness between the microchips.[50,51] In the center of each chip, a thin electron transparent membrane of 10–100 nm thickness provides a viewing window. When the liquid cell is placed in the vacuum of the electron microscope, these windows bulge outward typically by more than 0.5 µm each, which is often much larger than what is set by the spacer. The local thickness can be calculated from a model of the bulging.[61] The windows of the two chips can be aligned to provide parallel or crossed windows, depending on the users' requirements on the window dimension and liquid thickness. The closed cell can be glued to form a static cell[66] or clamped into a special liquid specimen holder by O-rings to make a flow cell.[50,59]

Flow cell and associated liquid flow holder designs allow for replenishing or changing of the solution chemistry in the cell while imaging, and have several other advantages. For example, many chemical reactions are triggered by introducing reactants to the solution. The ability to flow liquid in

LP-EM makes it possible to control the onset of the reaction at a desired location. This is particularly important for the real-time study of the dynamics of soft matter upon application of external stimuli, such as pH and temperature fluctuations. Generally, flow cells can be divided into bypass flow cells and direct flow cells. These two cell types have distinct differences in mass transfer properties during flow. For the bypass flow cell (Figure 3d), the injected liquid flows around the chips as well as between them. Each flow path has a certain flow resistance, and the flow through each channel follows linear scaling laws similar to those of parallel resistors carrying an electrical current,[50] as long as the flow channel is wetted and not too thin. The advantage of this geometry is a rapid exchange of the fluid of the whole flow system including supply lines to the outside of the microscope and a rapid change of the liquid between the windows. However, when the gap between the microchips gets too small, clogging may occur. Furthermore, there is a difference between liquid exchange in the middle between the windows and the liquid directly at the window surfaces, which can be exceptionally slow due to the bulging of windows leaving a bubble-shaped flow path with fast liquid exchange only in the middle.[67] Liquid exchange then occurs via slow diffusion from the flowing liquid in the middle to the almost still standing liquid at the window. If the spacer becomes thinner than 0.5 μm, mass transport may become too slow due to flow resistance. In a direct-flow cell (Figure 3e), the pressure can be increased in the flow channel between the windows so that liquid exchange can be forced even for very thin gaps.[51] The flushing of supply lines takes a long time in this case.

2.2.3. Graphene Liquid Cells

Other materials than SiN are used as well to make closed, of which encapsulation between two graphene sheets is the most popular (Figure 3f).[21] A GLC contains typically several tens of nanometers thick static, liquid pockets.[21] GLCs are known for their high-resolution imaging in LP-EM[23] as a consequence of the thin liquid layer and the negligible amount of electron scattering in the liquid-enclosing layer. Further advantages of graphene are its excellent thermal and electrical conductivity, and mechanical properties. Of practical advantage is that a GLC mounted in a 3 mm grid fits a standard TEM holder. It was also reported that graphene can act as radical quencher, thus reducing the radiation damage imposed on the sample.[68] A GLC was observed exhibiting about an order of magnitude higher dose tolerance than biomaterials imaged in cryo-TEM.[10b]

Different transfer methods for graphene have been developed as needed to construct a GLC.[21] One option is the so-called loop-assisted transfer method in which the graphene is deposited from a droplet captured in a loophole. The transfer method has been applied to enclose samples biomolecules in droplets of sizes mainly between 100 and 300 nm.[69] Graphene is also useful for covering larger objects such as whole cells immobilized on a substrate (Figure 3g).[52] Various other thin film or 2D materials can be used as well, such as carbon, boron nitride (h-BN), and MoS_2.

However, the main ongoing experimental challenge with GLCs is the reproducibility of making liquid pockets with a sufficiently large volume of liquid, and controlling the exact chemical content of the liquid.[21] A further practical problem has been limited and varied quality of the graphene. For example, certain batches contain flakes too small in size, or are contaminated with polymer-coating residues used in the transfer process of the graphene. A new method is to mount graphene on a support structure with holes (Figure 3h).[53,70] This new design of GLCs produces precisely controlled volumes of liquid and allows for nanometer-resolution elemental mapping on nanoparticles in liquid.

2.2.4. Liquid Cells for SEM

Although this progress report focuses on TEM and STEM, it should be mentioned that several systems have also been developed for SEM. The main advantage is that the large sample chamber of the SEM provides significant design freedom. One option is placing a soft matter sample in water in a capsule enclosed with a polymer membrane to obtain signal via backscattered electrons.[48] Placing the detector above the sample removes the necessity for thin liquid layers and hence mitigates the effects of confinement encountered in a standard liquid cell. Liquid cells for STEM in SEM have been developed.[71] It is also possible to combine an SEM with light microscopy in a system using a cell culture dish with a SiN membrane at the bottom.[72] With SEM in an upright configuration, the sample can be probed from below via backscattered electrons. SEM with an environmental chamber, so-called ESEM, allows liquid samples to be imaged when the temperature and the pressure in the vacuum chamber match the vapor pressure of the liquid.[73] Further advantages of SEM are the ability to include a 360° tilting stage [74] or a light microscope in the specimen chamber.[74,75]

2.2.5. Advanced Ways of Liquid Mixing

Mixing two solutions is perhaps the most common and most simple way to initiate a reaction in the laboratory, yet this remains a challenge in LP-EM. Dedicated experimental solutions have been developed to gain control of solution mixing. Most commercial LP-EM flow holders are capable of performing liquid mixing. A mixing liquid cell was used to study calcium carbonate nucleation by flowing $NaHCO_3$ and $CaCl_2$ into the cell with a liquid flow holder, using inlet/outlet lines.[76] Gas vapor can also be diffused into the microfluidic chamber to start a similar reaction.[77] A three-step diffusion method was introduced to perform solvent mixing in a bypass liquid cell starting a polymer self-assembly process (**Figure 4**a).[3b] In this case, the polymer solution was first flowed into the liquid cell, then vapor was used to expel the remaining polymer solution in the tubing, and finally, water was flowed in the liquid cell to initiate the assembly process.

However, with the current standard liquid flow specimen holders it is impossible to determine the extent of mixing inside the cell, as mixing often occurs in the space around the chips instead of in the viewing area. Improved control of liquid mixing may be achieved by using ultra-low volume

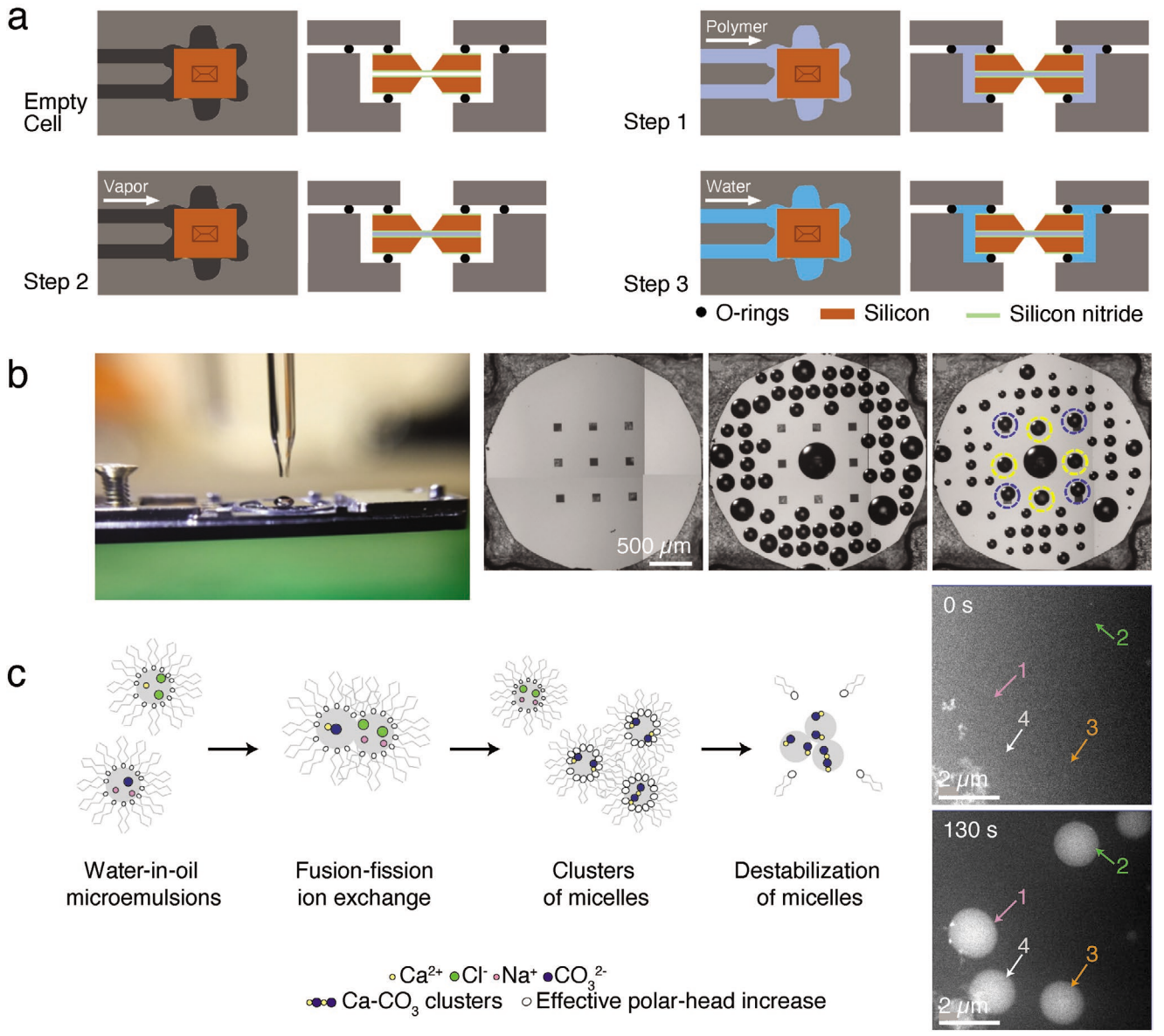

Figure 4. Advanced ways of liquid mixing. a) A three-step solvent mixing method allowed gradual increase of water content in a bypass cell system filled with a polymer solution.[3b] The polymer solution was first flowed in to fill the liquid cell, then the solvent vapor expelled the remaining polymer solution in the tubing, and finally, water was flowed in to start the self-assembly reaction. b) An ultralow volume dispenser was able to accurately load a certain volume of liquid onto the bottom chip. It applied a pattern of picoliter droplets from multiple solutions on the SiN surface of a microchip, thereby controlling the local mixing.[26,78] This system was used to deposit pure water droplets on a microchip with multiple windows. Afterward, 20 nm diameter gold nanoparticles (yellow) and 200 nm diameter metal–organic-framework nanoparticles (blue) were loaded.[78] c) A schematic showing how water-in-oil microemulsions can be used to carry Ca^{2+} and CO_3^{2-} in the liquid cell during flow, and are mixed through intermicellar exchange processes forming a stabilized solute $CaCO_3$ phase. The crystallization of solid $CaCO_3$ can be initiated "on demand" by the injection of ethanol to destabilize micelles carrying $CaCO_3$ solute.[79] The STEM images at the right side show the formation of large globules only after mixing of the two microemulsions which were carrying Ca^{2+} and CO_3^{2-} in the liquid cell. a) Adapted with permission.[3b] Copyright 2019, Springer Nature. b) Left panel: Reproduced with permission.[26] Copyright 2018, ACS. Other panels in (b): Reproduced with permission.[78] Copyright 2016, Cambridge University Press. c) Adapted with permission.[79] Copyright 2018, PCCP Owner Society.

liquid dispensing devices[78] or by employing nano/microsized polymer vehicles.[79] With the assistance of an automated piezoelectric-actuated dispenser, picoliter liquid droplets from different solutions were patterned into predefined arrays on the chip window, and mixing was initiated upon assembly of the top chip of the cell (Figure 4b).[78] Since the entire liquid loading process was automated by a robot, consistently thin liquid layers with predefined thickness, as well as similar liquid mixing conditions were obtained for each liquid cell, thus improving the reproducibility of the LP-EM experiments.[26] Water-in-oil microemulsions have been used as vehicles to carry different precursor ions, e.g., Ca^{2+} and CO_3^{2-} ions, in the

liquid cell during flow, such that the reaction can be somewhat slowed down or prevented due to the presence of a micellar interface (Figure 4c).[79] The formation of solid $CaCO_3$ can be initiated "on demand" by the injection of ethanol to destabilize micelles carrying the $CaCO_3$ solute.[79]

2.2.6. Microscope Innovations

LP-EM benefits from technical developments in electron optics, detectors, and acquisition methodologies. These advances allow researchers to monitor soft matter processes in multiple dimensions with fewer electrons, and improve spatial-temporal resolution. Spherical aberration correction in TEM and STEM has improved the spatial resolution for metallic samples to sub-Ångstrom, reduced delocalization, decreased the depth of field, and improved the interpretability of the obtained images.[1g] However, as spherical aberration correction only improves contrast for Ångstrom-sized features, the technique is typically not effective in LP-EM of soft matter, where radiation sensitivity of the materials prohibits such resolutions. Chromatic aberration correction,[80] on the other hand, is expected to be beneficial because it improves the balance of elastically scattered electrons focused in an image, and inelastically scattered electrons, which cannot be focused without this correction. Thus with aberration correction, it becomes possible to improve resolution at a given electron dose further,[44] and, in addition, facilitate imaging of thicker samples,[44,81] enable low voltage TEM at atomic resolution such to avoid knock-on damage.[82]

A third important innovation in the electron optics is the so-called phase plate for TEM.[83] With such a device, it is possible to obtain higher contrast than conventional TEM phase contrast. A phase plate increases the contrast by a factor of five for the relevant resolution range of 1–10 nm on biological material, as demonstrated experimentally.[84]

Another method for reducing the required electron dose while retaining the resolution is increasing the detection quantum efficiency (DQE) of the electron detection device. DQE is a performance metric defined as[85]

$$\mathrm{DQE} = \frac{\mathrm{SNR}^2_{\mathrm{output}}}{\mathrm{SNR}^2_{\mathrm{input}}} \tag{3}$$

Hence, when the DQE of a camera is improved by a factor of two, only a 25% electron dose is required to achieve the same image quality. Compared to the charge coupled devices (CCDs), direct electron detectors offer a significantly improved DQE over a much wider spectral range.[86] Their capability of fast readout and electron counting enables both high-speed acquisition and correction of image blurring due to sample dynamics at subpixel accuracy. Furthermore, it is possible to use a dose fractionation readout mode, which allows users to add and align an arbitrary number of sub-frames to access intermediate results during the sample imaging.[87] This is particularly interesting for imaging soft matter in liquid, as the onset of beam-induced sample damage can be precisely determined with this strategy,[1g] so that advanced processing techniques for 3D analysis referred to as Brownian tomography,[88] and single particle analysis[89] come into scope.

Another viable method for improving the resolution-dose balance is via intelligent image acquisition schemes that distribute electrons spatially and temporally to the most interesting sample locations at specific times. For example, imaging only where or when a sample region is changing most, referred to as adaptive sampling,[90] seems a reasonable strategy to be implemented, thereby dramatically reducing the applied total electron dose. Alternatively, by employing compressive sensing or sparse imaging in STEM using custom scan generators and/or fast beam blankers, the number of scanned pixels and thus the total dose can be reduced, while image information is recovered, e.g., by image inpainting.[91] Furthermore, the same approach can be used to increase the acquisition speed by more than an order of magnitude without replacing existing detectors.[92] This is also an effective way of reducing the amount of experimental data, particularly for high frame rate imaging. The combination of either phase-contrast TEM or STEM differential phase contrast[93] with adaptive and/or sparse sampling may turn out to be advantageous for an optimized dose-resolution balance for soft matter LP-EM.

Lastly, STEM acquisition using pixelated detectors are now becoming available such that optimized STEM differential phase contrast and ptychography[94] are additional options although solutions need to be found for the slow pixel-dwell time (sub-millisecond). Furthermore, as the phase information of the electron wave is sensitive to electric and magnetic fields, unique sample information such as charge distributions with high relevance to LP-EM may become obtainable.[95]

Time-resolved microscopy can be accomplished via direct imaging. State-of-the-art TEM cameras surpass millisecond frame rates, while STEM functions up to video frequency.[67] Alternatively, the electron source itself can be pulsed, e.g., by a laser. The electron column of dynamic TEM (DTEM) is optimized for pulses of high beam current thus obtaining snapshot images of processes in the sub-microsecond time regime.[96] By synchronizing sample excitation with the electron source triggered by a delayed laser pulse, ultrahigh temporal resolution is obtained, down to single-electron packets at the sample in femtoseconds,[97] which may also be achieved via ultrafast beam blanking.[98] So-called 4D TEM has been successfully applied in LP-EM to study rotational and translational dynamics of gold nanoparticles.[99] Importantly, 4D TEM has the ability to initiate reactions in the liquid cell by creating local pH and thermal changes, and is also able to induce photo-activated conformation changes or photo-induced nanoparticle growth.[100] In principle, the time evolution of radiation damage mechanisms in soft matter can also be studied at the sub-millisecond time-range using DTEM and beyond using 4D TEM.[99a,101]

3. Insights Offered by LP-EM

This section will show examples of how LP-EM has been used to study a variety of soft matter systems in both materials science and biology. LP-EM of soft-matter structure will be discussed on the basis of selected publications demonstrating what is possible in the field. We will discuss the strength of LP-EM in obtaining insight on the dynamics of selected systems through the direct observation of processes.

3.1. Imaging the Structure of Soft Matter in Liquid

Recent advances in low-dose LP-EM have initiated new research aimed at resolving the structure of soft matter in liquid at the nanoscale with different strategies including decreasing the thickness of the liquid layer and the window membrane[29b] as well as using heavy metal or particle labels.[3a,59,102] Nevertheless, it should be mentioned that imaging native biological structures in liquid with electron microscopy has a long history and was previously accomplished using environmental systems in TEM.[28,103]

3.1.1. The Need for Studying Structure in Liquid

For various forms of soft matter from either biological or synthetic origin, such as DNA, proteins, colloids, and polymers, their function and performance are related to their structure and morphology in the liquid state. Here, water plays an important role in stabilizing the secondary and tertiary conformation of proteins, and should therefore be regarded as an essential component for the structuring of soft matter.[104] Currently, cryo-TEM is an important tool for directly examining soft matter structures by making snapshots of samples embedded in amorphous vitrified ice.[105] Since the binding energies involved in the stabilization of the tertiary structure in soft mater structures are of a magnitude similar to the thermal energy at room temperature, these structures continuously experience Brownian motions due to thermal fluctuations in liquid. The structure–function relationship may thus be much more complex than suggested by the static conformations obtained from cryo-TEM or X-ray crystallography. Multiple configurations may play an important role, as well as their interchangeability. LP-EM offers a way to look directly at a soft matter system in a liquid environment, and thus to detect these multiple conformations and the way they interconvert.

3.1.2. Synthetic Soft Materials

Synthetic macromolecular structures have been directly imaged in liquid cells with SiN windows by modulation of the solvent composition in a flow cell. It has been possible to observe in situ the formation of the polymer bilayer membranes, of which the thickness was found to be similar to those of vesicles synthesized in bulk solution (**Figure 5**a). The membrane structures of polymer vesicles were observed of both pre-formed and as-synthesized vesicles in a flow cell with a low electron flux of 0.3 e^{-} $Å^{-2}$ s^{-1}.[3b]

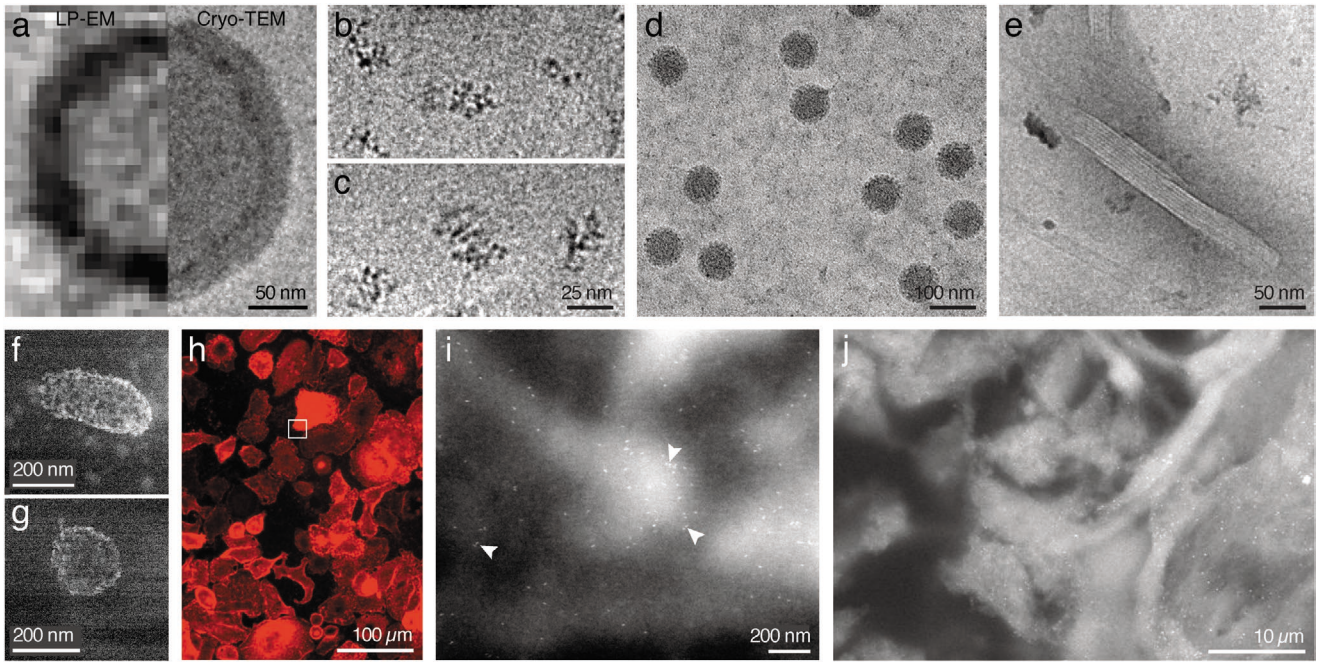

Figure 5. LP-EM of structures of soft matter in solution. a) Comparison of a polymer vesicle formed in the LP-EM (left) with a typical vesicle self-assembled in the bulk solution as analyzed by cryo-TEM (right).[3b] b,c) Representative TEM images showing individual poly(ethylene oxide) (top) and polystyrene sulfonate polymer molecules (bottom) in deionized water encapsulated by GLCs.[106] d) LP-EM of double-layered virus particles with viral mRNA transcripts.[111a] e) TEM image recording a microtubule encapsulated between two graphene sheets for which a higher dose tolerance was observed than for cryo-TEM.[10b] f,g) Different morphologies of cell-derived extracellular vesicles. Staining with gold nanoparticles was applied to enhance the contrast in STEM.[117] h) Fluorescence overview image of quantum dot-labeled HER2 proteins in SKBR3 human breast cancer cells.[3a] i) STEM in environmental SEM image of the boxed region in (h). Detected quantum dot labels appear as bright spots. Many pairs of HER2 are visible, examples are pointed out by arrowheads, representing signaling active homodimers. j) Distribution of cathepsin K in femur spongy bone in solution imaging using atmospheric SEM. Immuno-gold labeled Cathepsin K is visible as bright spots.[121] a) Reproduced with permission.[125] Copyright 2019, Springer Nature. b,c) Reproduced with permission.[106] Copyright 2017, Wiley-VCH. d) Reproduced with permission.[111a] Copyright 2015, RSC. e) Reproduced with permission.[10b] Copyright 2018, ACS. f,g) Reproduced with permission.[117] Copyright 2018, RSC. h,i) Adapted with permission.[3a] Copyright 2015, The Authors, published by AAAS. j) Adapted under the terms of the CC-BY Creative Commons Attribution 4.0 International License (http://creativecommons.org/licenses/by/4.0/).[121] Copyright 2019, The Authors, published by Springer Nature.

A flow cell was furthermore used to visualize hydrated globules of a poly styrene/Ca^{2+} complex employing a total dose of 50–300 e^{-} $Å^{-2}$, and to study subsequent diffusion of CO_2 to form $CaCO_3$, mimicking the initiation of crystal growth in mollusk shells.[77]

With their ability to mitigate radiation damage, GLCs exhibit great potential in the direct structural observation of macromolecules. GLC pockets were employed to visualize single polystyrene sulfonate and poly(ethylene oxide) macromolecules with nanometer resolution without labeling with metal particles.[106] Under these conditions, it was possible to directly observe the polymer globules and their size dependence on molecular weight and salt concentration (Figure 5b,c). Importantly, it was also found that when dissolved in D_2O, the lifetime under electron beam irradiation of the macromolecular structures was two to five times longer than in H_2O,[16] offering additional options for the direct observation of low contrast soft matter.

3.1.3. Biological Structure

Several early LP-EM experiments explored imaging of biological materials, such as bacteria,[107] eukaryotic cells,[59,62] and proteins.[108] SiN liquid cells were used to study the ultrastructure of fully hydrated, unfixed yeast cells without labeling or staining at a resolution of ≈30 nm (Figure 2b,c).[27] Others imaged naturally occurring magnetic nanoparticles in bacteria of the *Magnetospirillum magneticum* strain[109] and even visualized the magnetic induction map of these nanoparticles using off-axis holography.[110]

In several cases, advanced liquid cell designs were key for controlling the trapped liquid thickness and in visualizing the structure of biological soft matter. Unlabeled actin filaments in water were visualized at 2.7 nm resolution using SiN membranes of only 10 nm thick.[29b] Further, micelles, liposomes, and viral assemblies were studied using a SiN membrane patterned with wells (Figure 5d).[111] However, it should be noted that the obtained spatial resolution was exceptionally high and is possibly explained by the presence of a gas bubble created by electron-beam irradiation of the liquid.[62] A very thin liquid cell, created by sealing colloid-templated nanoscale cavities between two carbon films, was used to image the Y-shape of unstained antibodies at a spatial resolution of 2 nm.[112]

GLCs have become gradually more prevalent in biological structural determination in the liquid state. TEM visualization of enclosed bacteria was the first case of GLC-based imaging of biological materials.[113] Subsequent examples involved the imaging of proteins such as ferritins,[114] and eukaryotic cells.[115] Enclosure between graphene sheets of a hydrated microtubule sample (Figure 5e) has been reported to achieve an order of magnitude higher dose tolerance than what is known for cryo-TEM.[10b] Additionally, GLCs correlative light and electron microscopy has been used for the study of actin filaments, and protein distributions in eukaryotic cells.[52,116]

3.1.4. Labeling with Nanoparticles

Application of materials of high atomic number can enhance the contrast of soft matter in liquid of micrometers thickness, which is thick enough to study relevant samples, such as lipid vesicles, micelles, and whole cells. For example, Pt-containing micelles were synthesized for better liquid phase imaging contrast.[102a] The morphology of cell-derived extracellular vesicles was studied, which were circulating in body fluids. A controlled growth of gold nanoparticles on the vesicles was used to enhance their contrast in ADF STEM (Figure 5f,g).[117] In the biological field, gold nanoparticles were used for the study of nanoparticle uptake by eukaryotic cells in several micrometers of liquid with STEM.[102b] Already in the 1990s, gold-labeled myosin heads in muscle filaments were imaged in a hydration chamber in TEM.[103] The labeling of proteins with metal nanoparticles has been used to study cellular function with LP-EM in the past decade. For example, 4 nm spatial resolution was achieved when imaging gold-tagged macromolecules bound to the corresponding epidermal growth factor receptors of the cell through 7 ± 1 μm buffer solution.[59] Correlative fluorescence and LP-EM have become possible[118] with the use of fluorescent quantum dot nanoparticles[119] as specific protein labels. These have been used to visualize the local distribution of HER2 membrane proteins in breast cancer cells with a 3 nm spatial resolution.[3a] The functional state of HER2 proteins was determined from their presence either as signaling active homodimer or as inactive monomer (Figure 5h,i). This study led to the discovery that signaling active HER2 homodimers preferentially resided in ruffled membrane structures associated, which is relevant for understanding the mechanisms behind cancer metastasis development. LP-EM was thus used to study drug effects on HER2 overexpressing breast cancer.[120] Calcium phosphate mineralization in bone tissues has also been investigated via direct observation in aqueous media (Figure 5j).[121] Immuno-gold labeling was employed to highlight the localization of cathepsin K on the bone tissue.

LP-EM provides a much higher resolution for studying membrane proteins within intact cells than what is achievable in practice with super resolution fluorescence microscopy.[122] It is thus possible to study protein function via examining the stoichiometry of protein complexes.[122] Protein labeling was also used to examine calcium channels[48,72,123] and for axonal partitioning in primary-culture neurons.[124]

3.1.5. 3D Structure Visualization

Imaging the 3D structure of soft matter, particularly biological macromolecules such as proteins in aqueous liquid, is important for understanding their function and interaction in their native state. LP-EM offers an option for 3D structure analysis in liquid, and could develop into a new and complementary tool to cryo-TEM and X-ray crystallography in structural biology. With LP-EM, it is possible to obtain 3D structural information in three ways: 1) by using electron tomography,[88b,126] 2) by performing single particle analysis (3D averaging),[89] and 3) by applying electron diffraction tomography.[127] In LP-EM tomography, the 3D structure can be derived from conventional tilt series, as was done to study host–pathogen interactions.[88a] Since the samples are in liquid, LP-EM also offers an alternative method to image encapsulated nanoparticles that are rotating freely in liquid.[88b] If the trapped nanoparticles in liquid cell are

homogenous, such as purified viruses and proteins, the same single particle analysis method as used for cryo-TEM[128] can be employed in LP-EM to classify, align, and average the images of thousands of single particles to eventually reconstruct the 3D structure. It is also possible to examine how the 3D structures evolve over time by performing dynamic reconstruction, as demonstrated for ferritin.[89] When the observed specimen in liquid is crystalline, electron diffraction tomography techniques are also applicable for structural determination.[129] GLCs are probably the best choice for 3D LP-EM on account of the thin liquid layer, compatibility with the tomography holders, the available high tilt range, and radiation damage mitigation.

3.1.6. Dose Considerations when Studying Biological Systems

As the high-energy electrons used for imaging unavoidably damage the materials under investigation and alter the local solution chemistry, this external disturbance may greatly affect the entire system under investigation, leading to reorganization of the observed structures.[130,131] Even an electron dose of 1 e^{-} $Å^{-2}$ is already above the lethal dose for cells.[9] Thus, one of the key experimental concerns for the visualization of both chemical and biological soft matter is to determine whether LP-EM observations represent native structures, or structures induced by the electron beam. One useful measure for biological structures is to determine the extent to which the biological functions are preserved under the electron beam, where claims of viable systems should be supported by appropriate biological control experiments.[130] However, a window of opportunity is available by studying biochemical reactions under physiological conditions at highly optimized TEM or STEM settings. A recent example is the demonstration of enzymatic activity in experiments conducted in low-dose experiments.[31] Additionally, LP-EM observations can be validated by comparing with cryo-TEM results and thus establishing the electron radiation damage criteria.

3.2. Capturing the Dynamics of Soft Matter

Two primary challenges of accurately capturing dynamic process are controlling the system's dynamics inside the liquid cell, and optimizing the imaging conditions so that an appropriate temporal resolution can be achieved, while maintaining a minimum SNR as needed to observe the sample.[1g,h] Despite those experimental challenges, LP-EM has been used for the observation of dynamic phenomena integral to the development soft matter, including 1) translational and rotational motion, 2) conformational changes in biological macromolecules, and 3) self-assembly mechanisms of synthetic soft matter.

3.2.1. Translational and Rotational Motion

Understanding translational and rotational behavior of soft matter inside a liquid cell is of interest for studying nanoparticle motion in confined complex environments, and is also essential for making structural measurements and observing self-assembly mechanisms. In bulk liquid, nanoparticle movement obeys normal, Brownian motion. However, in confined/complex environments, such as the liquid cell, particles deviate from this behavior showing anomalous diffusion as a result of heterogeneities, entrapment, crowding, and con finement.[15a,67,131] Soft matter particle motion in liquid cells was initially studied by analyzing particle step velocity, or mean squared displacements versus time.[56,132] This analysis showed that motion was significantly reduced from the one in the bulk solution, as measured by nanoparticle tracking analysis or dynamic light scattering.[132a] The stochastic mechanisms behind anomalous diffusion, e.g., continuous time random walk or sub diffusive fractional Brownian motion, can be analyzed by the anomalous diffusion object motion analysis' method.[131] This is important as the mechanisms behind the motion are a reflection of the forces acting on the particles in solution and can provide a better understanding of the behind the dynamic processes. Anomalous diffusion is a common observation in liquid cell experiments,[133] e.g., the micelle motion in the liquid cell (**Figure 6**a),[3c] and is likely due to strong interactions between the particles and the surface of the liquid cell. However, it should be noted that particles moving with velocities that greatly exceed the frame rate and with step sizes that exceed the imaging area would be missed during any analysis, as millisecond imaging or faster would be needed.[134]

3.2.2. Conformational Changes in Biological Molecules

Understanding conformational changes in biological macromolecules, also known as the protein folding problem,[135] is a long standing grand scientific challenge. Although great progress has been made, there are still numerous questions to be answered where a direct observation of protein dynamics would make a significant contribution. Proteins are characterized by four levels of structural hierarchy, primary, secondary, tertiary, and quaternary structure. Thus far, LP-EM has only been applied to monitoring the evolution in quaternary structure, which is the assembly of multiple individual proteins into larger structures, due to the technical challenges associated with obtaining sufficient temporal and spatial resolution.[3d,136] For instance, LP-EM was used to study the nucleation and growth of lysozyme crystals (Figure 6b).[30a] Two types of amorphous particles facilitating nucleation of the crystals were identified by their observed dynamics: amorphous solid particles and noncrystalline particles. Although amorphous precursor particles have been well studied in protein crystallization, the mechanistic details of how one phase converts into another have not been well documented as this requires dynamic observations at the level of individual protein molecules.

Analogous to proteins, DNA also has four levels of structural arrangements. Using GLCs, the whole molecule kinetic conformation process of DNA from single strands to secondary structure, i.e., double helices, was monitored.[137] Multiple metastable intermediate structures were observed in the hybridization process, among which some have been predicted earlier before, e.g., contact zipper-up for random sequence (Figure 6c), and unanticipated frequent loop intermediates were also present to facilitate this process. These examples above represent the

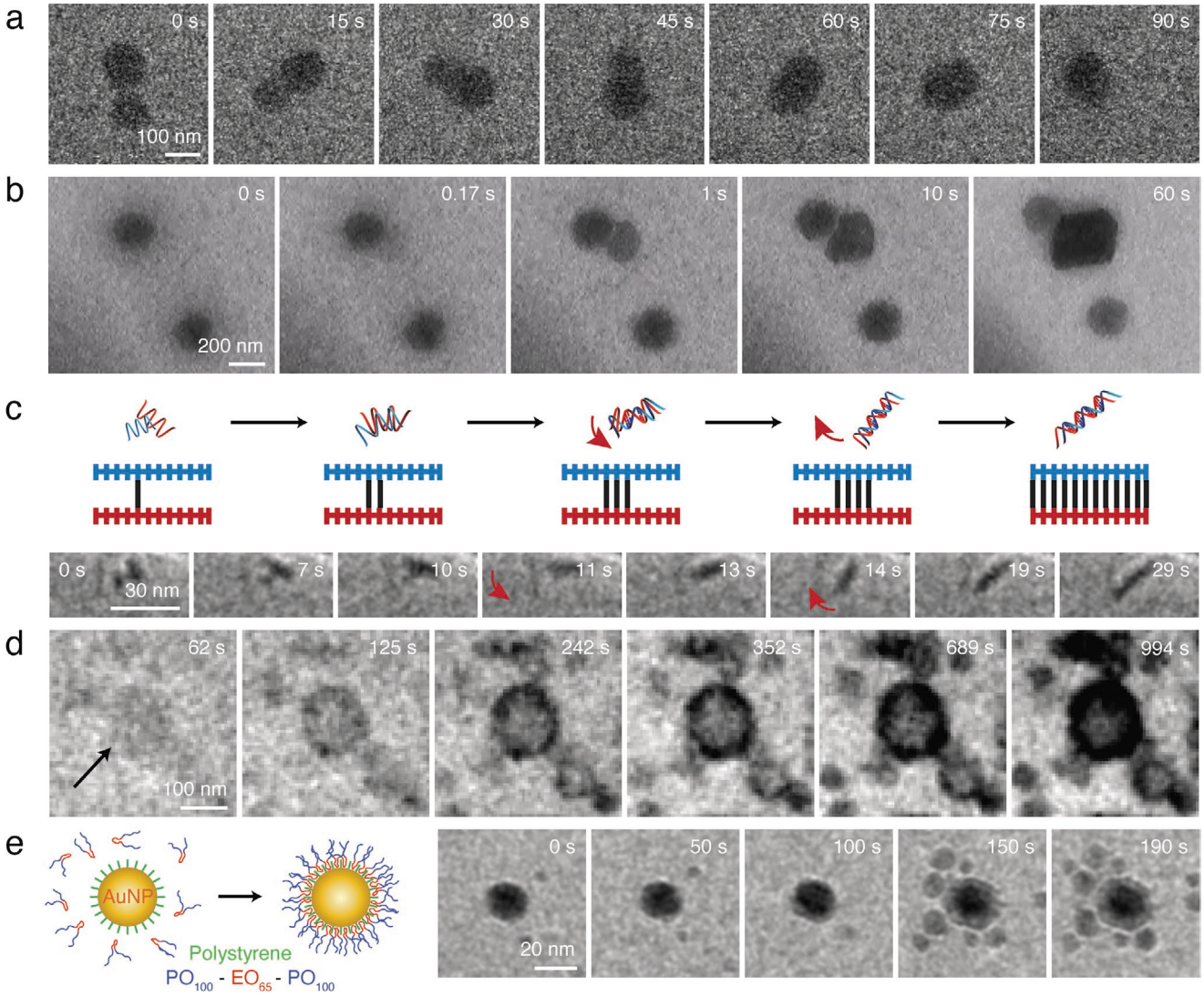

Figure 6. LP-EM of dynamics of soft matter in solution. a) Time-lapse LP-EM images of the fusion-relaxation process between two amphiphilic block copolymer micelles.[3c] b) Nucleation process of lysozyme crystals monitored by LP-EM, showing a protein crystal formed near an amorphous solid particle.[30a] c) A DNA zipper-up hybridization process imaged by LP-EM. This mechanism was initiated by contact of bases located near the middle of strands (0, 7, and 10 s). Arrows at 11 and 14 s present different rotation directions. Top view: schematic diagrams of time-dependent conformations. Second row: schematics showing the base-pair alignment. Third row: actual images.[137] d) LP-EM showing the block copolymer vesicle formed through the nucleation of a polymer-rich liquid droplet highlighted by the black arrow.[125] e) Direct imaging of encapsulation process of gold NPs with the triblock copolymers.[3e] a) Adapted with permission.[3c] Copyright 2017, ACS. b) Adapted with permission.[30a] Copyright 2017, The Authors, published by National Academy of Sciences, USA. c) Adapted with permission.[137] Copyright 2020, The Authors, published by National Academy of Sciences, USA. d) Adapted with permission.[3b] Copyright 2019, Springer Nature. e) Adapted with permission.[3e] Copyright 2019, RSC.

important role of LP-EM in contributing to the understanding of conformational changes in biological macromolecules.

3.2.3. Self-Assembly of Synthetic Soft Matter

The self-assembly of synthetic soft materials occurs at various levels of hierarchy where an analogy exists to the primary, secondary, tertiary, and quaternary of biological macromolecules. The motion of individual polystyrene sulfonate and poly(ethylene oxide) chains with a radius of gyration of 30–50 nm was visualized using GLCs, demonstrating that LP-EM has the potential to contribute to understanding the folding of individual macromolecules.[106] Understanding chain folding dynamics is crucial in polymer self-assembly, as it determines important features of the hierarchical structures, such as the diameter of spherical or cylindrical micelles and the thickness of vesicle membranes. The latter has been investigated using a combination of LP-EM and self-consistent mean field theory simulations (Figure 6d).[3b] The thickness of the vesicle membrane was shown to be determined by two dynamic processes, the insertion of chains into the vesicle and the reorganization of the individual chains from a coiled to stretched configuration. The combination of these methods provided a

platform for differentiating between the thermodynamic and kinetic components in the self-assembly. It also revealed that the onset of the kinetic pathways in the vesicle formation process was influenced by the formation of a polymer-rich liquid droplet (62 s, Figure 6d) prior to membrane self-assembly. LP-EM played an important role by determining the mechanistic connection between these phases.

LP-EM is also well suited for studying how soft matter particles interact mechanistically. Soft matter fusion processes have been observed for both low[3e] and high[3c] glass transition temperature T_g polymer assemblies. In both cases, fusion processes were observed occurring simultaneously with unimer addition, gradual attachment of individual polymer chains. In the case of the low T_g system, the fusion events had no influence on the morphology evolution (Figure 6e). In the high T_g system, the fusion events were found to result in the entrapment of internal water phase within the assemblies leading to increased internal structural complexity typically associated with high genus and bi-continuous structures (Figure 6a). This is consistent with the concept that low T_g polymers can easily form low energy configurations at room temperature, and consequently display a pathway-independent morphology, whereas high T_g polymers are more likely to form meta-stable or out-of-equilibrium structures and be pathway-dependent.[138] However, LP-EM enabled the direct observation of these processes for the first time, and in the high T_g case, provided the first direct evidence of how the process of fusion can be used to control morphology (Figure 6a).

In the above examples, self-assembly was triggered by either mixing solutions inside the microscope,[3b] mechanical agitation of the system during loading,[3c] or pre-mixing solutions before loading into the cell.[3d,3e] One of the main challenges here is to control the onset of self-assembly at a desired location and time. In the study of inorganic nanocrystal formation by LP-EM, such control is commonly achieved by using the electron beam to initiate the reaction, providing a tight control over the nucleation and growth chemistry.[11b] This approach was extended to the study of soft matter systems by using the electron beam to initiate radical polymerizations inside the liquid cell and study the process of polymerization-induced self-assembly.[26] As this is a widely applied method for the generation of polymer nanoparticles in bulk solution, it is an ideal system for study using LP-EM, especially if the polymerization kinetics can be controlled by varying the applied dose to the sample.

For completeness, it should be mentioned that the definition of soft matter could also be extended beyond materials consisting purely of soft matter and include also hard matter, e.g., metal nanoparticles bound by weak bonds in a matrix in liquid. LP-EM is an excellent tool for studying self-assembly processes of those quasi-soft materials.[10a,139]

4. Outlook

We see exciting future opportunities for LP-EM in studying both the dynamic evolution of morphology and structure of complex molecular systems in solution. Indeed, understanding the interactions between different components in solution will allow us to both understand the science behind the interactions and create new assemblies with well-defined shapes, sizes, and chemistries that self-organize into functional, hierarchical structures for a variety of (bio)technological applications, and find new clues in biomedical sciences possibly leading to improved therapies against cancer, e.g. To obtain this level of information via LP-EM experiments, beam effects need to be understood and avoided as much as possible, while control and comparing experiments should be conducted so as to obtain evidence that the obtained information reliably visualizes processes that occur in the real world, i.e., outside the electron microscope. While recognizing the explorative nature of the research in the past decade, a more systematic approach in LP-EM experiment is needed to enhance further growth of the field and solve a wide range of research question using this technique. As a starting point for LP-EM experiments, we recommend following the schematic shown in **Figure 7** to evaluate whether or not LP-EM can be expected to be useful and feasible for the type of research question to be addressed, and how to choose the most optimal experimental settings.

A key feature of these experiments is the nanoscale confinement of the sample. While the effect of confinement on motion has been explored through studies of translation and rotational motion, detailed studies as a function of particle size and shape, type of medium, and surface characteristics are still required. These studies should include, but are not limited to, varying particle parameters as well as window electrostatics and conductivity in combination with the solution's Debye length, and varying in the Van der Walls interactions between particle, solution, and windows. Such studies would not only provide valuable insight for applications of soft matter to nanomedicine where particles must travel through complex confined environments, but would also aid the design of LP-EM experiments to study self-assembly mechanisms. For example, in studying processes such as particle assembly or fusion, it is essential that the particle translation dynamics are sufficient to result in a statistically significant number of particle–particle collisions. Studies of the formation of individual particles can be aided by having the particles permanently adhered to the windows to limit motion blur. Although such studies have been reported, there have been no examples of LP-EM studies where dynamics have been designed a priori.

From the perspective of imaging, a very promising approach is the development of imaging strategies with ultra-low electron doses using sparse imaging. Although mostly applied in STEM imaging, sparse imaging was recently also applied to TEM in a proof-of-concept study, using a pixelated detector at a very high frame rate and very low dose.[92] In addition, the recent advances in phase plate technology,[83,140] so far mainly demonstrated in cryo-TEM applications, boost the contrast (at resolutions > 1 nm), thereby further reducing the number of electrons needed to obtain the same image quality.

To judge if a process is indeed being visualized without significantly changing their outcome or kinetics, knowledge is required of the chemical composition of the solution under imaging conditions as well as the temperature, either through modeling or continuous monitoring. Eventually, all relevant solution conditions would need to be known and regulated by measuring and controlling temperature, pH, and the concentration of all reactants. A potential solution to achieve this

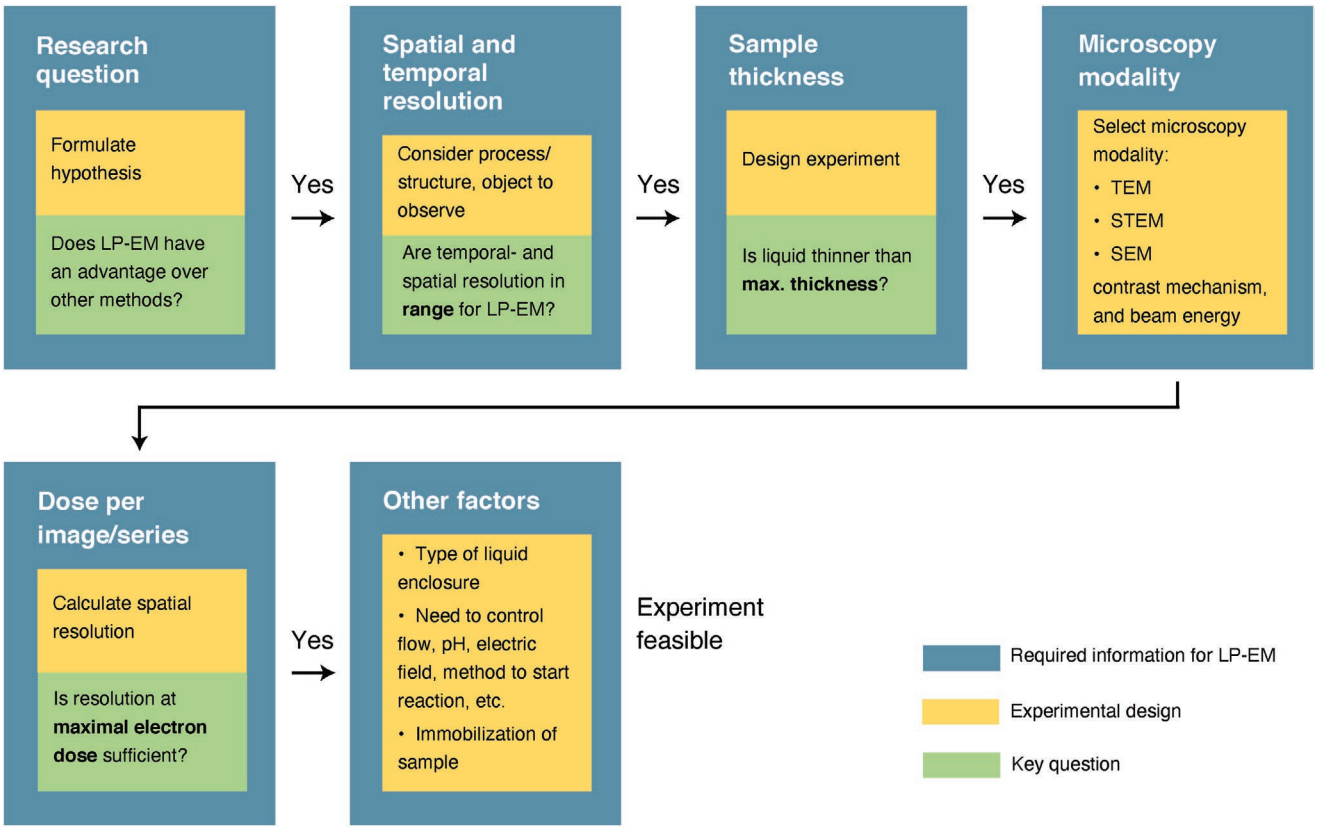

Figure 7. Schematic to evaluate the feasibility of LP-EM experiment and to determine the most optimal experimental settings. It is recommended that LP-EM is benchmarked with other techniques first, then to check if the observables are within the resolution range addressed by LP-EM, i.e., a spatial resolution typically of 1–10 nm, and a temporal range of 0.01–100 s, whereby the range can be extended using technological advances. A critical question is whether the system to be observed in its full functional state is thin enough to be studied with LP-EM, e.g., the maximal thickness for ADF STEM with a useful resolution is 10 µm, while phase-contrast TEM requires the sample to be thinner than 300 nm. The different electron microscopy types and contrast mechanisms need to be evaluated against the required resolution and sample thickness. Once these choices have been made, the dose-limited spatial resolution can be calculated from which it can then be determined if the experiment is feasible in terms of electron dose. Finally, a range of other important experimental factors need to be considered.

high level of control is the development of liquid holders with connections for temperature control (measuring and heating), and the ability to measure/adjust pH and chemical potentials, possibly in connection with modeling software to correlate the values measured at the detectors with those in the imaging area. In another approach toward obtaining information about the liquid constituents, the feasibility of post-imaging mass spectrometry has been demonstrated,[31] and such analysis could possibly be developed into a method for online analysis of the solution, which would allow for the adjustment of imaging conditions to safeguard chemical integrity of the components under study.

Using the electron beam to trigger reactions offers interesting possibilities for the study of electrochemical processes in soft matter, considering the growing interest in the use of conductive,[141] or electrically responsive soft materials.[142] Interesting examples are the so-called "e-micellization," involving the electrochemical induction and switching of the aggregation of polymers,[143] the electrochemical formation of layered titanate microspherulite particles,[144] and the redox-dependent reversible formation of pickering emulsions.[145] Another exciting topic could be the investigation of hybrid electronics for their application in lithium batteries,[146] where specifically electro-polymerization reactions of conducting polymers are an area of great interest.[147] In general, we think that the renewed interest in electrochemistry and electrocatalysis as green synthesis methods will allow numerous applications for LP-EM to monitor morphological and structural development in situ. In particular, the high energy and flux of the electrons used in electron microscopy offers a unique type of electrical stimulation, which is not currently used in flask-based chemistry. In this scenario, LP-EM of soft materials may be used for blue-skies research for discovery of unique structure and chemistries.

So far LP-EM has been mainly used to study the dynamics of inorganic and metal nanoparticle systems in solution, and only a limited number of studies have investigated reactions occurring in soft organic materials, while the use of LP-EM to study biological processes is virtually unexplored. However, the recent demonstration that below a certain threshold level biomacromolecules enclosed within a GLC are an order of magnitude more resistant to radiation damage than frozen samples for cryo-TEM[10b,11b] brings into scope the dynamic nanoscale imaging of biomolecular processes with LP-EM. Moreover, a recently developed simple, reliable, and reproducible procedure

allows the production of GLCs with sizes of 100–2000 nm.[69] As graphene can be easily surface-modified with a great variety of chemical moieties, this will offer the possibility of capturing and retaining biomolecules and biomolecular assemblies in a closed, near-native environment. It may also be possible to make a graphene liquid flow cell, which is capable of sustained liquid flow and can be electrically contacted.[148] We expect that these recent developments will bring us another step toward the dynamic in situ imaging of soft matter and biological processes with spatial and temporal resolutions that are unobtainable with other methods such as with super-resolution microscopy and cryo-TEM.

5. Summary and Conclusions

Radiation damage is a key factor to consider when performing LP-EM experiments with soft matter. Depending on the type of research question, a different limit on the total dose and electron flux may apply. Experimental settings should optimize the needed resolution rather than the maximal resolution of a specific materials system in the minimum required liquid thickness within the dose limit. The dose "history" should be accurately reported, and dead time during the experiment should be accounted for. The liquid thickness should be measured and reported. Different microscopy modalities and liquid enclosures can be chosen based on the type of experiment. A GLC combined with phase contrast TEM achieves the highest resolution, but a flow cell with SiN windows and STEM may be the best for observing certain dynamic reactions. A broad range of soft matter systems has been studied with LP-EM including lipid vesicles, biominerals, polymer nanoparticles, virus particles, and bacterial, yeast, and eukaryotic cells. The obtained resolution varied between a few nanometers for thin samples to several tens of nanometers depending on the liquid thickness. The main driver for developing LP-EM is to progress in the understanding of structure–function relationships. Function in soft matter nowadays is often explained on the basis of a few static conformations as obtained, e.g., with cryo-TEM, although dynamics in morphology is possibly a key factor in important self-assembly processes and biological function. Moreover, LP-EM can be a much simpler experiment than cryo-TEM, and opens up the capability to study materials in a broad range of liquids.

Here, we have discussed that dynamic processes can be directly viewed when the experimental system is well controlled and the electron irradiation is kept below an acceptable level. Although several examples have already been published, e.g., the fusion-relaxation process between two amphiphilic block copolymer micelles, huge potential exists for future improvements. In order to address biochemical reactions, the required dose for a time-lapse image series needs to be reduced by three orders of magnitude. This seems feasible by combining the recent innovations in liquid cells, dose mitigation approaches, intelligent data acquisition techniques, and highly efficient detection using phase plate technology, e.g. LP-EM has already come a long way mainly due to technological improvement of the liquid enclosing membranes using either SiN or graphene windows. An exciting future lies ahead for this microscopy modality in which greatly improved technology can be expected together with key progress in solving grand challenges in soft matter research and biology.

Acknowledgements

The authors acknowledge T. Trampert for help with the figures, and P. Kunnas for help with Figure 1, writing drafts of several paragraphs, and discussions. E. Arzt is acknowledged for his support through INM. Funding was provided by the EU H2020 Marie Sklodowska-Curie Action project "MULITMAT" (676045).

Conflict of Interest

The authors declare no conflict of interest.

Keywords

beam–sample interactions, dynamic processes, in situ electron microscopy, synthetic materials

Received: March 5, 2020
Revised: April 5, 2020
Published online: May 17, 2020

[1] a) N. de Jonge, F. M. Ross, *Nat. Nanotechnol.* **2011**, *6*, 695; b) T. Ngo, H. Yang, *J. Phys. Chem. Lett.* **2015**, *6*, 5051; c) H.-G. Liao, H. Zheng, *Annu. Rev. Phys. Chem.* **2016**, *67*, 719; d) B. H. Kim, J. Yang, D. Lee, B. K. Choi, T. Hyeon, J. Park, *Adv. Mater.* **2018**, *30*, 1703316; e) F. M. Ross, *Science* **2015**, *350*, aaa9886; f) J. J. De Yoreo, N. A. J. M. Sommerdijk, *Nat. Rev. Mater.* **2016**, *1*, 16035; g) N. de Jonge, L. Houben, R. E. Dunin-Borkowski, F. M. Ross, *Nat. Rev. Mater.* **2019**, *4*, 61.

[2] H. Zheng, R. K. Smith, Y. W. Jun, C. Kisielowski, U. Dahmen, A. P. Alivisatos, *Science* **2009**, *324*, 1309.

[3] a) D. B. Peckys, U. Korf, N. de Jonge, *Sci. Adv.* **2015**, *1*, e1500165; b) A. Ianiro, H. Wu, M. M. J. van Rijt, M. P. Vena, A. D. A. Keizer, A. C. C. Esteves, R. Tuinier, H. Friedrich, N. Sommerdijk, J. P. Patterson, *Nat. Chem.* **2019**, *11*, 320; c) L. R. Parent, E. Bakalis, A. Ramirez-Hernandez, J. K. Kammeyer, C. Park, J. de Pablo, F. Zerbetto, J. P. Patterson, N. C. Gianneschi, *J. Am. Chem. Soc.* **2017**, *139*, 17140; d) T. Yamazaki, Y. Kimura, P. G. Vekilov, E. Furukawa, M. Shirai, H. Matsumoto, A. E. Van Driessche, K. Tsukamoto, *Proc. Natl. Acad. Sci. USA* **2017**, *114*, 2154; e) C. Li, C. C. Tho, D. Galaktionova, X. Chen, P. Kral, U. Mirsaidov, *Nanoscale* **2019**, *11*, 2299.

[4] a) S. A. P. van Rossum, M. Tena-Solsona, J. H. van Esch, R. Eelkema, J. Boekhoven, *Chem. Soc. Rev.* **2017**, *46*, 5519; b) D. M. Marolf, M. R. Jones, *Anal. Chem.* **2019**, *91*, 13324; c) M. Nguyen, S. Vaikuntanathan, *Proc. Natl. Acad. Sci. USA* **2016**, *113*, 14231.

[5] a) Y. Yan, J. Huang, B. Z. Tang, *Chem. Commun.* **2016**, *52*, 11870; b) J. van der Gucht, *Front. Phys.* **2018**, *6*, 87.

[6] C. A. S. Batista, R. G. Larson, N. A. Kotov, *Science* **2015**, *350*, 1242477.

[7] F. M. Ross, *Liquid Cell Electron Microscopy*, Cambridge University Press, Cambridge, UK **2017**.

[8] R. F. Egerton, *Micron* **2019**, *119*, 72.

[9] L. Reimer, H. Kohl, *Transmission Electron Microscopy: Physics of Image Formation*, Springer, New York **2008**.

[10] a) S. Keskin, S. Besztejan, G. Kassier, S. Manz, R. Bucker, S. Riekeberg, H. K. Trieu, A. Rentmeister, R. J. Miller, *J. Phys. Chem. Lett.* **2015**, *6*, 4487; b) S. Keskin, N. de Jonge, *Nano Lett.* **2018**, *18*, 7435; c) M. Wang, C. Park, T. Woehl, *Microsc. Microanal.* **2019**, *25*, 23.
[11] a) N. M. Schneider, M. M. Norton, B. J. Mendel, J. M. Grogan, F. M. Ross, H. H. Bau, *J. Phys. Chem.* **2014**, *118*, 22373; b) T. J. Woehl, P. Abellan, *J. Microsc.* **2017**, *265*, 135.
[12] H. Su, B. L. Mehdi, J. P. Patterson, N. A. Sommerdijk, N. D. Browning, H. Friedrich, *J. Phys. Chem. C* **2019**, *123*, 25448.
[13] S. M. Ghodsi, S. Anand, R. Shahbazian-Yassar, T. Shokuhfar, C. M. Megaridis, *ACS Nano* **2019**, *13*, 4677.
[14] J. Hermannsdoerfer, N. de Jonge, A. Verch, *Chem. Commun.* **2015**, *51*, 16393.
[15] a) H. Zheng, S. A. Claridge, A. M. Minor, A. P. Alivisatos, U. Dahmen, *Nano Lett.* **2009**, *9*, 2460; b) J. M. Grogan, N. M. Schneider, F. M. Ross, H. H. Bau, *Nano Lett.* **2014**, *14*, 359; c) Z. Aabdin, X. M. Xu, S. Sen, U. Anand, P. Kral, F. Holsteyns, U. Mirsaidov, *Nano Lett.* **2017**, *17*, 2953.
[16] H. Wang, K. H. Nagamanasa, Y.-J. Kim, O.-H. Kwon, S. Granick, *ACS Nano* **2018**, *12*, 8572.
[17] T. H. Moser, H. Mehta, C. Park, R. T. Kelly, T. Shokuhfar, J. E. Evans, *Sci. Adv.* **2018**, *4*, eaaq1202.
[18] R. F. Egerton, P. Li, M. Malac, *Micron* **2004**, *35*, 399.
[19] Y. Liu, X.-M. Lin, Y. Sun, T. Rajh, *J. Am. Chem. Soc.* **2013**, *135*, 3764.
[20] B. L. Mehdi, A. Stevens, L. Kovarik, N. Jiang, H. Mehta, A. Liyu, S. Reehl, B. Stanfill, L. Luzi, W. Hao, L. Bramer, N. D. Browning, *Appl. Phys. Lett.* **2019**, *115*, 063102.
[21] M. Textor, N. de Jonge, *Nano Lett.* **2018**, *18*, 3313.
[22] S. M. Rehn, M. R. Jones, *ACS Energy Lett.* **2018**, *3*, 1269.
[23] J. M. Yuk, J. Park, P. Ercius, K. Kim, D. J. Hellebusch, M. F. Crommie, J. Y. Lee, A. Zettl, A. P. Alivisatos, *Science* **2012**, *336*, 61.
[24] M. Wang, C. Park, T. J. Woehl, *Chem. Mater.* **2018**, *30*, 7727.
[25] P. Abellan, T. H. Moser, I. T. Lucas, J. W. Grate, J. E. Evans, N. D. Browning, *RSC Adv.* **2017**, *7*, 3831.
[26] M. A. Touve, C. A. Figg, D. B. Wright, C. Park, J. Cantlon, B. S. Sumerlin, N. C. Gianneschi, *ACS Cent. Sci.* **2018**, *4*, 543.
[27] D. B. Peckys, P. Mazur, K. L. Gould, N. De Jonge, *Biophys. J.* **2011**, *100*, 2522.
[28] V. R. Matricardi, R. C. Moretz, D. F. Parsons, *Science* **1972**, *177*, 268.
[29] a) T. H. Moser, T. Shokuhfar, J. E. Evans, *Micron* **2019**, *117*, 8; b) U. M. Mirsaidov, H. Zheng, Y. Casana, P. Matsudaira, *Biophys. J.* **2012**, *102*, L15.
[30] a) T. Yamazaki, Y. Kimura, P. G. Vekilov, E. Furukawa, M. Shirai, H. Matsumoto, A. E. S. Van Driessche, K. Tsukamoto, *Proc. Natl. Acad. Sci. USA* **2017**, *114*, 2154; b) J. P. Patterson, P. Abellan, M. S. Denny, C. Park, N. D. Browning, S. M. Cohen, J. E. Evans, N. C. Gianneschi, *J. Am. Chem. Soc.* **2015**, *137*, 7322.
[31] M. A. Touve, A. S. Carlini, N. C. Gianneschi, *Nat. Commun.* **2019**, *10*, 4837.
[32] a) H. Stark, F. Zemlin, C. Boettcher, *Ultramicroscopy* **1996**, *63*, 75; b) B. E. Bammes, J. Jakana, M. F. Schmid, W. Chiu, *J. Struct. Biol.* **2010**, *169*, 331; c) J. F. Conway, B. L. Trus, F. P. Booy, W. W. Newcomb, J. C. Brown, A. C. Steven, *J. Struct. Biol.* **1993**, *111*, 222.
[33] S. B. Hayward, R. M. Glaeser, *Ultramicroscopy* **1979**, *4*, 201.
[34] P. N. T. Unwin, R. Henderson, *J. Mol. Biol.* **1975**, *94*, 425.
[35] a) P. Abellan, T. J. Woehl, L. R. Parent, N. D. Browning, J. E. Evans, I. Arslan, *Chem. Commun.* **2014**, *50*, 4873; b) T. J. Woehl, K. L. Jungjohann, J. E. Evans, I. Arslan, W. D. Ristenpart, N. D. Browning, *Ultramicroscopy* **2013**, *127*, 53; c) J. Hermannsdörfer, V. Tinnemann, D. B. Peckys, N. de Jonge, *Microsc. Microanal.* **2016**, *22*, 656.
[36] N. de Jonge, *Ultramicroscopy* **2018**, *187*, 113.
[37] K. Gnanasekaran, G. de With, H. Friedrich, *R. Soc. Open Sci.* **2018**, *5*, 171838.
[38] A. Rose, *Vision: Human and Electronic*, Plenum Press, New York **1973**.
[39] T. Schuh, N. de Jonge, *C. R. Phys.* **2014**, *15*, 214.
[40] J. E. Evans, N. D. Browning, *J. Electron Microsc.* **2013**, *62*, 147.
[41] M. Vulović, R. B. G. Ravelli, L. J. van Vliet, A. J. Koster, I. Lazić, U. Lücken, H. Rullgård, O. Öktem, B. Rieger, *J. Struct. Biol.* **2013**, *183*, 19.
[42] H. Demers, N. Poirier-Demers, A. R. Couture, D. Joly, M. Guilmain, N. De Jonge, D. Drouin, *Scanning* **2011**, *33*, 135.
[43] K. L. Klein, I. M. Anderson, N. de Jonge, *J. Microsc.* **2011**, *242*, 117.
[44] J. P. Baudoin, J. R. Jinschek, C. B. Boothroyd, R. E. Dunin-Borkowski, N. de Jonge, *Microsc. Microanal.* **2013**, *19*, 814.
[45] N. de Jonge, N. Poirier-Demers, H. Demers, D. B. Peckys, D. Drouin, *Ultramicroscopy* **2010**, *110*, 1114.
[46] D. B. Peckys, J. P. Baudoin, M. Eder, U. Werner, N. de Jonge, *Sci. Rep.* **2013**, *3*, 2626.
[47] A. Bogner, G. Thollet, D. Basset, P. H. Jouneau, C. Gauthier, *Ultramicroscopy* **2005**, *104*, 290.
[48] S. Thiberge, A. Nechushtan, D. Sprinzak, O. Gileadi, V. Behar, O. Zik, Y. Chowers, S. Michaeli, J. Schlessinger, E. Moses, *Proc. Natl. Acad. Sci. USA* **2004**, *101*, 3346.
[49] a) M. F. Hohmann-Marriott, A. A. Sousa, A. A. Azari, S. Glushakova, G. Zhang, J. Zimmerberg, R. D. Leapman, *Nat. Methods* **2009**, *6*, 729; b) M. Elbaum, S. G. Wolf, L. Houben, *MRS Bull.* **2016**, *41*, 542; c) S. G. Wolf, L. Houben, M. Elbaum, *Nat. Methods* **2014**, *11*, 423.
[50] E. A. Ring, N. de Jonge, *Microsc. Microanal.* **2010**, *16*, 622.
[51] C. Mueller, M. Harb, J. Dwyer, R. D. Miller, *J. Phys. Chem. Lett.* **2013**, *4*, 2339.
[52] I. N. Dahmke, A. Verch, J. Hermannsdorfer, D. B. Peckys, R. S. Weatherup, S. Hofmann, N. de Jonge, *ACS Nano* **2017**, *11*, 11108.
[53] D. J. Kelly, M. Zhou, N. Clark, M. J. Hamer, E. A. Lewis, A. M. Rakowski, S. J. Haigh, R. V. Gorbachev, *Nano Lett.* **2018**, *18*, 1168.
[54] D. R. G. Mitchell, M. J. B. Nancarrow, *Microsc. Res. Tech.* **2015**, *78*, 886.
[55] A. S. Kashin, V. P. Ananikov, *Nat. Rev. Chem.* **2019**, *3*, 624.
[56] A. Verch, M. Pfaff, N. De Jonge, *Langmuir* **2015**, *31*, 6956.
[57] R. Kroger, A. Verch, *Minerals* **2018**, *8*, 21.
[58] K. L. Jungjohann, J. E. Evans, J. A. Aguiar, I. Arslan, N. D. Browning, *Microsc. Microanal.* **2012**, *18*, 621.
[59] N. de Jonge, D. B. Peckys, G. J. Kremers, D. W. Piston, *Proc. Natl. Acad. Sci. USA* **2009**, *106*, 2159.
[60] a) H. R. Zhang, R. F. Egerton, M. Malac, *Micron* **2012**, *43*, 8; b) M. E. Holtz, Y. Yu, J. Gao, H. D. Abruna, D. A. Muller, *Microsc. Microanal.* **2013**, *19*, 1027.
[61] S. Keskin, P. Kunnas, N. de Jonge, *Nano Lett.* **2019**, *19*, 4608.
[62] D. B. Peckys, G. M. Veith, D. C. Joy, N. de Jonge, *PLoS One* **2009**, *4*, e8214.
[63] I. Pereiro, A. Fomitcheva Khartchenko, L. Petrini, G. V. Kaigala, *Lab Chip* **2019**, *19*, 2296.
[64] U. M. Mirsaidov, H. Zheng, D. Bhattacharya, Y. Casana, P. Matsudaira, *Proc. Natl. Acad. Sci. USA* **2012**, *109*, 7187.
[65] a) I. M. Abrams, J. W. McBain, *J. Appl. Phys.* **1944**, *15*, 607; b) E. Ruska, *Kolloid-Z.* **1942**, *100*, 212.
[66] M. J. Williamson, R. M. Tromp, P. M. Vereecken, R. Hull, F. M. Ross, *Nat. Mater.* **2003**, *2*, 532.
[67] E. A. Ring, N. de Jonge, *Micron* **2012**, *43*, 1078.
[68] H. Cho, M. R. Jones, S. C. Nguyen, M. R. Hauwiller, A. Zettl, A. P. Alivisatos, *Nano Lett.* **2017**, *17*, 414.
[69] P. M. G. van Deursen, R. I. Koning, V. Tudor, M.-A. Moradi, J. P. Patterson, A. Kros, N. A. J. M. Sommerdijk, A. J. Koster, G. F. Schneider, *Adv. Funct. Mater.* **2020**, *30*, 1904468.

[70] A. Hutzler, T. Schmutzler, M. P. M. Jank, R. Branscheid, T. Unruh, E. Spiecker, L. Frey, *Nano Lett.* **2018**, *18*, 7222.
[71] J. M. Grogan, N. M. Schneider, F. M. Ross, H. H. Bau, *J. Indian Inst. Sci.* **2012**, *92*, 295.
[72] H. Nishiyama, M. Suga, T. Ogura, Y. Maruyama, M. Koizumi, K. Mio, S. Kitamura, C. Sato, *J. Struct. Biol.* **2010**, *169*, 438.
[73] D. L. Stokes, *Principles and Practice of Variable Pressure/Environmental Scanning Electron Microscopy (VP-SEM)*, Wiley, Chichester, UK **2008**.
[74] K. Masenelli-Varlot, A. Malchere, J. Ferreira, H. Heidari Mezerji, S. Bals, C. Messaoudi, S. Marco Garrido, *Microsc. Microanal.* **2014**, *20*, 366.
[75] N. Liv, A. C. Zonnevylle, A. C. Narvaez, A. P. Effting, P. W. Voorneveld, M. S. Lucas, J. C. Hardwick, R. A. Wepf, P. Kruit, J. P. Hoogenboom, *PLoS One* **2013**, *8*, e55707.
[76] M. H. Nielsen, S. Aloni, J. J. De Yoreo, *Science* **2014**, *345*, 1158.
[77] P. J. M. Smeets, K. R. Cho, R. G. E. Kempen, N. Sommerdijk, J. J. De Yoreo, *Nat. Mater.* **2015**, *14*, 394.
[78] J. P. Patterson, L. R. Parent, J. Cantlon, H. Eickhoff, G. Bared, J. E. Evans, N. C. Gianneschi, *Microsc. Microanal.* **2016**, *22*, 507.
[79] T. M. Stawski, T. Roncal-Herrero, A. Fernandez-Martinez, A. Matamoros-Veloza, R. Kröger, L. G. Benning, *Phys. Chem. Chem. Phys.* **2018**, *20*, 13835.
[80] M. Haider, P. Hartel, H. Muller, S. Uhlemann, J. Zach, *Philos. Trans. R. Soc., A* **2009**, *367*, 3665.
[81] N. J. Zaluzec, *Ultramicroscopy* **2015**, *151*, 240.
[82] M. Linck, P. Hartel, S. Uhlemann, F. Kahl, H. Muller, J. Zach, M. Haider, M. Niestadt, M. Bischoff, J. Biskupek, Z. Lee, T. Lehnert, F. Borrnert, H. Rose, U. Kaiser, *Phys. Rev. Lett.* **2016**, *117*, 076101.
[83] R. Danev, B. Buijsse, M. Khoshouei, J. M. Plitzko, W. Baumeister, *Proc. Natl. Acad. Sci. USA* **2014**, *111*, 15635.
[84] R. Danev, R. M. Glaeser, K. Nagayama, *Ultramicroscopy* **2009**, *109*, 312.
[85] R. R. Meyer, A. I. Kirkland, *Microsc. Res. Tech.* **2000**, *49*, 269.
[86] a) C. Booth, P. Mooney, *Microsc. Anal.* **2013**, *27*, 13; b) A. R. Farugi, R. Hernderson, G. McMullan, *Adv. Imaging Electron Phys.* **2015**, *190*, 103.
[87] X. Li, P. Mooney, S. Zheng, C. R. Booth, M. B. Braunfeld, S. Gubbens, D. A. Agard, Y. Cheng, *Nat. Methods* **2013**, *10*, 584.
[88] a) W. J. Dearnaley, B. Schleupner, A. C. Varano, N. A. Alden, F. Gonzalez, M. A. Casasanta, B. E. Scharf, M. J. Dukes, D. F. Kelly, *Nano Lett.* **2019**, *19*, 6734; b) J. Park, H. Elmlund, P. Ercius, J. M. Yuk, D. T. Limmer, Q. Chen, K. Kim, S. H. Han, D. A. Weitz, A. Zettl, *Science* **2015**, *349*, 290.
[89] G. Marchello, C. De Pace, N. Wilkinson, L. Ruiz-Perez, G. Battaglia, arXiv:1907.03348, **2019**.
[90] T. Dahmen, M. Engstler, C. Pauly, P. Trampert, N. de Jonge, F. Mucklich, P. Slusallek, *Sci. Rep.* **2016**, *6*, 25350.
[91] a) A. Stevens, H. Yang, L. Carin, I. Arslan, N. D. Browning, *Microscopy* **2014**, *63*, 41; b) A. Beche, B. Goris, B. Freitag, J. Verbeeck, *Appl. Phys. Lett.* **2016**, *108*, 093103.
[92] A. Stevens, L. Kovarik, P. Abellan, X. Yuan, L. Carin, N. D. Browning, *Adv. Struct. Chem. Imaging* **2015**, *1*, 10.
[93] I. Lazic, E. G. T. Bosch, S. Lazar, *Ultramicroscopy* **2016**, *160*, 265.
[94] Y. Jiang, Z. Chen, Y. Han, P. Deb, H. Gao, S. Xie, P. Purohit, M. W. Tate, J. Park, S. M. Gruner, V. Elser, D. A. Muller, *Nature* **2018**, *559*, 343.
[95] D. Wolf, R. Hubner, T. Niermann, S. Sturm, P. Prete, N. Lovergine, B. Buchner, A. Lubk, *Nano Lett.* **2018**, *18*, 4777.
[96] T. LaGrange, G. H. Campbell, B. Reed, M. Taheri, J. B. Pesavento, J. S. Kim, N. D. Browning, *Ultramicroscopy* **2008**, *108*, 1441.
[97] A. H. Zewail, *Science* **2010**, *328*, 187.
[98] W. Verhoeven, J. F. M. van Rens, A. H. Kemper, E. H. Rietman, H. A. van Doorn, I. Koole, E. R. Kieft, P. H. A. Mutsaers, O. J. Luiten, *Rev. Sci. Instrum.* **2019**, *90*, 083703.
[99] a) X. Fu, B. Chen, J. Tang, M. T. Hassan, A. H. Zewail, *Science* **2017**, *355*, 494; b) X. Fu, B. Chen, J. Tang, A. H. Zewail, *Sci. Adv.* **2017**, *3*, e1701160.
[100] J. E. Evans, K. L. Jungjohann, N. D. Browning, I. Arslan, *Nano Lett.* **2011**, *11*, 2809.
[101] E. J. VandenBussche, D. J. Flannigan, *Nano Lett.* **2019**, *19*, 6687.
[102] a) M. T. Proetto, A. M. Rush, M.-P. Chien, P. Abellan Baeza, J. P. Patterson, M. P. Thompson, N. H. Olson, C. E. Moore, A. L. Rheingold, C. Andolina, *J. Am. Chem. Soc.* **2014**, *136*, 1162; b) D. B. Peckys, N. de Jonge, *Nano Lett.* **2011**, *11*, 1733.
[103] H. Sugi, T. Akimoto, K. Sutoh, S. Chaen, N. Oishi, S. Suzuki, *Proc. Natl. Acad. Sci. USA* **1997**, *94*, 4378.
[104] F. M. Ross, *Liquid Cell Electron Microscopy*, Cambridge University Press, Cambridge **2016**.
[105] J. P. Patterson, Y. Xu, M.-A. Moradi, N. A. J. M. Sommerdijk, H. Friedrich, *Acc. Chem. Res.* **2017**, *50*, 1495.
[106] K. H. Nagamanasa, H. Wang, S. Granick, *Adv. Mater.* **2017**, *29*, 1703555.
[107] K. L. Liu, C. C. Wu, Y. J. Huang, H. L. Peng, H. Y. Chang, P. Chang, L. Hsu, T. R. Yew, *Lab Chip* **2008**, *8*, 1915.
[108] J. E. Evans, K. L. Jungjohann, P. C. K. Wong, P. L. Chiu, G. H. Dutrow, I. Arslan, N. D. Browning, *Micron* **2012**, *43*, 1085.
[109] T. J. Woehl, S. Kashyap, E. Firlar, T. Perez-Gonzalez, D. Faivre, D. Trubitsyn, D. A. Bazylinski, T. Prozorov, *Sci. Rep.* **2015**, *4*, 6854.
[110] T. Prozorov, T. P. Almeida, A. Kovacs, R. E. Dunin-Borkowski, *J. R. Soc., Interface* **2017**, *14*, 20170464.
[111] a) A. C. Varano, A. Rahimi, M. J. Dukes, S. Poelzing, S. M. McDonald, D. F. Kelly, *Chem. Commun.* **2015**, *51*, 16176; b) M. J. Dukes, R. Thomas, J. Damiano, K. L. Klein, S. Balasubramaniam, S. Kayandan, J. S. Riffle, R. M. Davis, S. M. McDonald, D. F. Kelly, *Microsc. Microanal.* **2014**, *20*, 338.
[112] C. Wadell, S. Inagaki, T. Nakamura, J. Shi, Y. Nakamura, T. Sannomiya, *ACS Nano* **2017**, *11*, 1264.
[113] N. Mohanty, M. Fahrenholtz, A. Nagaraja, D. Boyle, V. Berry, *Nano Lett.* **2011**, *11*, 1270.
[114] C. Wang, Q. Qiao, T. Shokuhfar, R. F. Klie, *Adv. Mater.* **2014**, *26*, 3410.
[115] J. Park, H. Park, P. Ercius, A. F. Pegoraro, C. Xu, J. W. Kim, S. H. Han, D. A. Weitz, *Nano Lett.* **2015**, *15*, 4737.
[116] M. Wojcik, M. Hauser, W. Li, S. Moon, K. Xu, *Nat. Commun.* **2015**, *6*, 7384.
[117] M. Piffoux, N. Ahmad, J. Nelayah, C. Wilhelm, A. Silva, F. Gazeau, D. Alloyeau, *Nanoscale* **2018**, *10*, 1234.
[118] M. J. Dukes, D. B. Peckys, N. de Jonge, *ACS Nano* **2010**, *4*, 4110.
[119] B. N. Giepmans, T. J. Deerinck, B. L. Smarr, Y. Z. Jones, M. H. Ellisman, *Nat. Methods* **2005**, *2*, 743.
[120] D. B. Peckys, U. Korf, S. Wiemann, N. de Jonge, *Mol. Biol. Cell* **2017**, *28*, 3193.
[121] C. Sato, D. Yamazaki, M. Sato, H. Takeshima, N. Memtily, Y. Hatano, T. Tsukuba, E. Sakai, *Sci. Rep.* **2019**, *9*, 7352.
[122] N. De Jonge, *J. Microsc.* **2018**, *269*, 134.
[123] a) D. Alansary, D. B. Peckys, B. A. Niemeyer, N. de Jonge, *J. Cell Sci.* **2020**, *133*, jcs240358; b) Y. Maruyama, T. Ebihara, H. Nishiyama, M. Suga, C. Sato, *J. Struct. Biol.* **2012**, *180*, 259; c) N. Liv, D. S. van Oosten Slingeland, J. P. Baudoin, P. Kruit, D. W. Piston, J. P. Hoogenboom, *ACS Nano* **2016**, *10*, 265.
[124] K. Hirano, T. Kinoshita, T. Uemura, H. Motohashi, Y. Watanabe, T. Ebihara, H. Nishiyama, M. Sato, M. Suga, Y. Maruyama, N. M. Tsuji, M. Yamamoto, S. Nishihara, C. Sato, *Ultramicroscopy* **2014**, *143*, 52.
[125] A. Ianiro, H. Wu, M. M. van Rijt, M. P. Vena, A. D. Keizer, A. C. C. Esteves, R. Tuinier, H. Friedrich, N. A. Sommerdijk, J. P. Patterson, *Nat. Chem.* **2019**, *11*, 320.
[126] W. Dearnaley, B. Schleupner, A. C. Varano, N. Alden, F. Gonzalez, M. Casasanta, B. E. Scharf, M. J. Dukes, D. F. Kelly, *Nano Lett.* **2019**, *19*, 6734.

[127] O. M. Karakulina, A. Demortière, W. Dachraoui, A. Abakumov, J. Hadermann, *Nano Lett.* **2018**, *18*, 6286.
[128] J. Frank, *Three-Dimensional Electron Microscopy of Macromolecular Assemblies: Visualization of Biological Molecules in Their Native State*, Oxford University Press, Oxford, UK **2006**.
[129] B. L. Nannenga, T. Gonen, *Nat. Methods* **2019**, *16*, 369.
[130] N. de Jonge, D. B. Peckys, *ACS Nano* **2016**, *10*, 9061.
[131] L. R. Parent, E. Bakalis, M. Proetto, Y. W. Li, C. Park, F. Zerbetto, N. C. Gianneschi, *Acc. Chem. Res.* **2018**, *51*, 3.
[132] a) M. T. Proetto, A. M. Rush, M. P. Chien, P. Abellan Baeza, J. P. Patterson, M. P. Thompson, N. H. Olson, C. E. Moore, A. L. Rheingold, C. Andolina, J. Millstone, S. B. Howell, N. D. Browning, J. E. Evans, N. C. Gianneschi, *J. Am. Chem. Soc.* **2014**, *136*, 1162; b) U. Mansfeld, S. Hoeppener, U. S. Schubert, *Adv. Mater.* **2013**, *25*, 761.
[133] S. W. Chee, U. Anand, G. Bisht, S. F. Tan, U. Mirsaidov, *Nano Lett.* **2019**.
[134] S. W. Chee, Z. Baraissov, N. D. Loh, P. T. Matsudaira, U. Mirsaidov, *J. Phys. Chem. C* **2016**, *120*, 20462.
[135] K. A. Dill, J. L. MacCallum, *Science* **2012**, *338*, 1042.
[136] H. Le Ferrand, M. Duchamp, B. Gabryelczyk, H. Cai, A. Miserez, *J. Am. Chem. Soc.* **2019**, *141*, 7202.
[137] H. Wang, B. Li, Y. J. Kim, O. H. Kwon, S. Granick, *Proc. Natl. Acad. Sci. USA* **2020**, *117*, 1283.
[138] D. B. Wright, J. P. Patterson, N. C. Gianneschi, C. Chassenieux, O. Colombani, R. K. O'Reilly, *Polym. Chem.* **2016**, *7*, 1577.
[139] a) Q. Chen, J. M. Smith, J. Park, K. Kim, D. Ho, H. I. Rasool, A. Zettl, A. P. Alivisatos, *Nano Lett.* **2013**, *13*, 4556; b) Z. Ou, Z. Wang, B. Luo, E. Luijten, Q. Chen, *Nat. Mater.* **2020**, *19*, 450.
[140] Y. Inayoshi, H. Minoda, Y. Arai, K. Nagayama, *Micron* **2012**, *43*, 1091.
[141] a) M. Kaltenbrunner, T. Sekitani, J. Reeder, T. Yokota, K. Kuribara, T. Tokuhara, M. Drack, R. Schwödiauer, I. Graz, S. Bauer-Gogonea, S. Bauer, T. Someya, *Nature* **2013**, *499*, 458; b) N. L. Ing, R. K. Spencer, S. H. Luong, H. D. Nguyen, A. I. Hochbaum, *ACS Nano* **2018**, *12*, 2652.
[142] W. A. Ogden, Z. Guan, *ChemSystemsChem* **2019**, *1*, e1900030.
[143] F. A. Plamper, L. Murtomäki, A. Walther, K. Kontturi, H. Tenhu, *Macromolecules* **2009**, *42*, 7254.
[144] Y. Tang, Y. Lai, D. Gong, K.-H. Goh, T.-T. Lim, Z. Dong, Z. Chen, *Chem. - Eur. J.* **2010**, *16*, 7704.
[145] L. Peng, A. Feng, S. Liu, M. Huo, T. Fang, K. Wang, Y. Wei, X. Wang, J. Yuan, *ACS Appl. Mater. Interfaces* **2016**, *8*, 29203.
[146] H. Wu, G. Yu, L. Pan, N. Liu, M. T. McDowell, Z. Bao, Y. Cui, *Nat. Commun.* **2013**, *4*, 1943.
[147] J. A. Arter, D. K. Taggart, T. M. McIntire, R. M. Penner, G. A. Weiss, *Nano Lett.* **2010**, *10*, 4858.
[148] V. P. Adiga, G. Dunn, A. K. Zettl, A. P. Alivisatos, *US20160042912A1*, **2016**.